

Flip dynamics in three-dimensional random tilings

V. Desoutter, N. Destainville

Laboratoire de Physique Théorique – IRSAMC
UMR 5152 CNRS/Université Paul Sabatier,
118, route de Narbonne, 31062 Toulouse Cedex 04, France.

Abstract. We study single-flip dynamics in sets of three-dimensional rhombus tilings with fixed polyhedral boundaries. This dynamics is likely to be slowed down by so-called “cycles”: such structures arise when tilings are encoded *via* the “partition-on-tiling” method and are susceptible to break connectivity by flips or at least ergodicity, because they locally suppress a significant amount of flip degrees of freedom. We first address the so-far open question of the connectivity of tiling sets by elementary flips. We prove exactly that sets of tilings of codimension one and two are connected for any dimension and tiling size. For higher-codimension tilings of dimension 3, the answer depends on the precise choice of the edge orientations, which is a non-trivial issue. In most cases, we can prove connectivity despite the existence of cycles. In the few remaining cases, among which the icosahedral symmetry, the question remains open. We also study numerically flip-assisted diffusion to explore the possible effects of the previously mentioned cycles. Cycles do not seem to slow down significantly the dynamics, at least as far as self-diffusion is concerned.

Key-words: Random tilings – Quasicrystals – Discrete dynamical systems – Connectivity – Diffusion.

1. Introduction

Rhombus tilings in dimensions 2 and 3 have been an interdisciplinary subject of intensive study in the two last decades, both in theoretical solid state physics because of their strong relation with quasicrystals [1, 2, 3], as well as in theoretical computer science or in more fundamental mathematics [4, 5, 6, 7, 8, 9, 10]. Rhombus tilings are coverings of a portion of Euclidean space, without gaps or overlaps, by rhombi in dimension two and rhombohedra in dimension three. The “cut-and-project” process is a standard method [2, 11] to generate such tilings. It consists in selecting sites and tiles in a D -dimensional cubic lattice and to project them onto a d -dimensional subspace with $D > d$; d is the dimension of the tilings and the difference $D - d$ is usually called their *codimension*. The class of symmetry of a tiling is related to D and d and such tilings will be denoted by $D \rightarrow d$ tilings. Icosahedral tilings that are widely studied in quasicrystal science, are $6 \rightarrow 3$ tilings of codimension 3. We consider in this paper three-dimensional tilings of codimensions ranging from 1 to 4. We also make incursions in the general $D \rightarrow d$ case whenever it is possible.

The “generalized partition” method used in this paper to generate tilings is a variant of the previous one which has proven useful in several circumstances to

manipulate and count them [12, 13, 14, 15, 7, 16, 17]. The principles of the method will be recalled below. However, we should already mention that the tilings generated by this technique have specific fixed boundaries. They are polygons in dimension 2 and polyhedra in dimension 3, all of them belonging to the class of *zonotopes* [18].

As compared to perfect quasiperiodic rhombus tilings, such as the celebrated Penrose tilings [4], the so-called “random tilings” [3] have additional degrees of freedom, the *localized phasons* or *elementary flips*, which consist of local rearrangements of tiles (groups of 4 tiles in dimension 3). The activation of these degrees of freedom gives rise to a large amount of accessible configurations which are responsible for a macroscopic configurational entropy, the calculation of which is in itself a difficult topic that the present paper does not address directly.

Among the many problems that remain unsolved in this field, results on flip-dynamics are scarce in three dimensions [19, 20, 21, 22, 23, 10] and are either purely numerical or based upon an approximate Langevin approach. And yet it is a crucial issue in quasicrystal science where elementary flips are believed to play an important role because they are a new source of atomic mobility. They could bring their own contribution to self-diffusion [24] in quasicrystalline alloys and they are involved in some specific mechanical properties, such as plasticity related to dislocation mobility [25] (see the introduction of section 6 for a more detailed discussion).

The present paper addresses two issues related to single-flip dynamics: connectivity of tiling sets *via* elementary flips and self-diffusion (of vertices) in random tilings when flips are activated.

The question of the connectivity of tiling sets *via* elementary flips still resists investigation in spite of the apparent simplicity of its formulation: *is it possible to reach any tiling from any other one by a sequence of elementary flips?* Even if proving that tiling sets are connected *via* elementary flips is only a first step towards the full characterization of flip dynamics, it is a challenging question that must imperatively be addressed before tackling more complex issues such as ergodicity, self-diffusion, calculation of ergodic times [26, 10] or dislocation mobility. This connectivity issue is also crucial in the context of Monte Carlo simulations on tilings: it is a fundamental ingredient if one hopes to sample correctly their configuration spaces.

So far, connectivity has only been conjectured by Las Vergnas about 25 years ago in the context of “oriented matroid theory” [27]. In two dimensions, connectivity can be established [5, 6], but the proofs are very specific to dimension 2 and cannot be adapted to dimensions 3 and higher. In reference [16], a new proof of the connectivity in dimension 2 was proposed and the reason why this proof could not be easily extended to higher dimensions was clearly identified: there appear “cycles” (defined below) in the generalized partition method which locally suppress a fraction of flip degrees of freedom. It is this point of view that we shall adopt in the present paper: we shall demonstrate that the obstacles to the generalization of the latter proof can be rigorously bypassed in many cases: in codimensions 1 and 2; in most cases in codimensions 3 and 4. We say “most cases” because a new difficulty arises when one studies three-dimensional rhombic tilings: for a given codimension, all edge orientations are not equivalent. There are 4 non-equivalent edge orientations in codimension 3 and 11 ones in codimension 4. The paper discusses this non-trivial issue in great detail. There is a minority of edge orientations where we are not able to prove connectivity. Note that when all edge orientations are not combinatorially equivalent, the corresponding polyhedral fixed boundaries are not topologically equivalent either. This point will also be discussed in great detail in the paper.

Beyond connectivity, the previously mentioned cycles are likely to affect ergodicity. Since they suppress some flip degrees of freedom, they are susceptible to slow down the dynamics and to be responsible for entropic barriers which could for instance prevent a tile from finding its average equilibrium position in the tiling. We have chosen to study self-diffusion of vertices to explore such possible effects. Self-diffusion has previously been studied in icosahedral tilings [21, 22, 23] but the effect of cycles themselves has never been investigated. We shall see that there are no significant difference in the diffusive behavior between tilings where cycles exist and those where we are able to prove that they cannot exist, nor between tilings where connectivity can be proven and those where it remains open. No sub-diffusive regimes at long time are observed whatever the tilings under consideration. Cycles do not seem to slow down the dynamics, at least as far as self-diffusion is concerned.

The paper is organized as follows: In section 2, we describe the “generalized partition” method used throughout the paper to code the tilings. In the following section 3, we set the basics of flip dynamics, we introduce “cycles”, and we discuss their possible influence on the dynamics by flips. Section 4 discusses the question of non-equivalent edge orientations and related fixed boundaries. In section 5, we prove that cycles cannot exist in favorable conditions, which enables us to prove connectivity by flips in a large variety of cases. In addition, we make a brief incursion into order theory: we prove that the tiling sets have a structure of “graded poset”. When cycles exist, we also study how abundant they are and we derive a simple mean-field argument to account for our observations. Finally, section 6 is devoted to a numerical study of the diffusion of vertices. The last section 7 contains conclusive remarks and open questions.

2. Tilings and generalized partitions

In this section, we introduce the concept of generalized partition used in the paper to code and manipulate rhombus tilings. This technique was introduced in [12, 13, 14], developed in [15, 16] and mathematically formalized in [7]. Our purpose here is not to give a rigorous presentation that can be found in these references, but rather to provide an intuitive view of the technique.

2.1. Generalities

The rhombus tilings considered in this paper, whatever their dimension, have D possible edge orientations (belonging to \mathbb{R}^d), denoted by e_a , $a = 1, \dots, D$. They are inherited from the D directions of the cubic lattice of \mathbb{R}^D during the “cut-and-project” process. Each possible edge has the orientation and norm of one of the vectors e_a . The signs of these vectors e_a are irrelevant and can be arbitrarily chosen. A rhombic tile is defined by d of these edge orientations. To avoid flat tiles, the family of orientation vectors is supposed to be *non-degenerate*: any d of them form a basis of \mathbb{R}^d .

A dual representation of rhombus tilings was introduced by de Bruijn [28, 29]. It consists in seeing the tiling as a grid of lines (see figure 2, right). A line in a tiling is a succession of adjacent tiles sharing an edge (in dimension 2) or a face (in dimension 3) with a given orientation. It is always possible to extend these lines through the whole tiling up to a boundary tile. These lines are called “de Bruijn lines”. In dimension 3, one can also define de Bruijn surfaces which can be represented by adjacent tiles sharing an edge with a given orientation e_a (see fig 1). They play the role of de Bruijn

lines in dimension 3. It exists one family of lines, or surfaces, denoted by F_a , for each orientation e_a of edges. There are p_a surfaces in the family F_a . De Bruijn surfaces of the same family do not intersect. A tiling with D orientations of edges on a d -dimensional space will be called a $D \rightarrow d$ tiling, and $D - d$ defines its codimension. In dimension d , the de Bruijn surfaces are replaced by $(d-1)$ -dimensional hyper-surfaces.

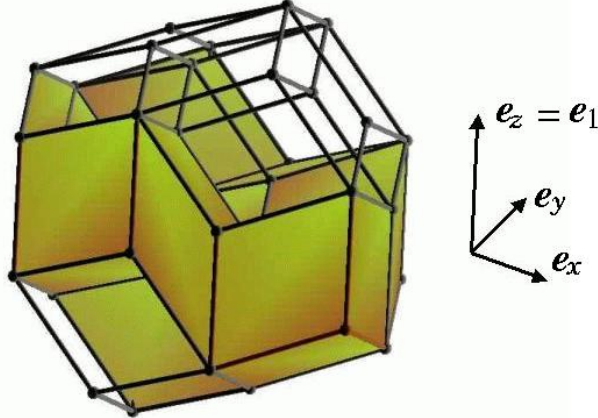


Figure 1. Unitary tiling with icosahedral symmetry. Shaded tiles form the de Bruijn surface attached to the edge orientation e_1 equal to e_z in this figure. This de Bruijn surface can be seen as a (mono-valued) function from $(xOy) = \mathbb{R}^2$ to $(Oz) = \mathbb{R}$. It is topologically equivalent to a $5 \rightarrow 2$ tiling with decagonal boundary.

In this paper, we will mainly be interested in the case $d = 3$, and we shall use 2-dimensional tiling examples to facilitate the comprehension. In dimension 3, a rhombic tile is given by the intersection of three surfaces of different families, and so all the different types of tiles are given by all the possible intersections of 3 surfaces of different families; there are $\binom{D}{3}$ different species of tiles. We can prolong any de Bruijn surface of family F_a beyond the tiling boundaries and up to infinity, by a surface perpendicular to the direction e_a far from the tiling. If the tiling corresponds to a complete grid, which means that any three surfaces of different families have a non-empty intersection, it will have fixed boundary conditions (see section 4). More precisely, this boundary will be a zonotope [18], that is to say the shadow of the hypercube of sides (p_1, p_2, \dots, p_D) in the D -dimensional space onto the d -dimensional space, where we recall that the p_a are the numbers of hyper-surfaces in family F_a . We shall discuss more precisely this kind of boundary in section 4.

Here we make an important remark about de Bruijn surfaces: a $(d-1)$ -dimensional de Bruijn surface S in a $D \rightarrow d$ tiling t_d is topologically equivalent to a $D-1 \rightarrow d-1$ tiling. For example, a de Bruijn surface in a 3-dimensional tiling can also be seen as a 2-dimensional tiling. Indeed, let us consider the trace on S of the d -dimensional de Bruijn grid dual of t_d : it is a grid made of $D-1$ families of $(d-2)$ -dimensional surfaces. This grid is complete because the original grid is. It is the dual of a $D-1 \rightarrow d-1$ tiling with fixed zonotopal boundaries. In figure 1, a de Bruijn surface is represented. The equivalent 2-dimensional rhombus tiling is obtained by looking at the surface from the direction e_z .

A tiling will be called “unitary” if it contains one de Bruijn line or surface per family ($p_a = 1$ for all a). It will be called “diagonal” if it contains the same number of de Bruijn lines or surfaces in each family ($p_a = p$ for all a).

2.2. Generalized partitions

Now the idea of the generalized partitions method is to build iteratively the tiling, by reconstructing the dual grid. In dimension 3, beginning with a complete grid made by only three families of surfaces, which is unique and represents a $3 \rightarrow 3$ periodic tiling made by one type of tiles, we have to describe where to place the de Bruijn surfaces of the fourth family F_4 relatively to the existing intersections of 3 surfaces. In terms of tilings, it means that we have to describe where to place the fourth surfaces of tiles on the existing $3 \rightarrow 3$ tiling. The resulting tiling will depend on where one places the surfaces of the fourth family relatively to the original grid. And iteratively, to build a $D+1 \rightarrow 3$ tiling, we have to describe where to place the family F_{D+1} of surfaces on a previously obtained $D \rightarrow 3$ tiling. In order to obtain a tiling by this process, we have to impose some constraints on the way we place the next family of surfaces at each step. The surfaces of one family cannot intersect. No more than 3 surfaces can cross at the same point, otherwise the tile at this point cannot be properly defined. Furthermore, de Bruijn surfaces are directed [15]. Indeed, by construction, they always cross edges with a given orientation, and can be seen as mono-valued functions $\mathbb{R}^{d-1} \rightarrow \mathbb{R}$ defined on the hyper-plane perpendicular to their orientation vector e_a (see figure 1).

Let us now introduce (see figure 2) how one can define a partial order relation between the tiles of a tiling in order to satisfy these constraints. Since the p_a de Bruijn surfaces of a family F_a do not intersect, they divide the space \mathbb{R}^d in $p_a + 1$ disjoint domains. Furthermore, since de Bruijn surfaces are globally oriented, we can index these domains from 0 to p_a such that, following the direction given by e_a we go through all these domains in an increasing order. We denote these domains by D_0, \dots, D_{p_a} and the surfaces of F_a by S_1, \dots, S_{p_a} . The de Bruijn surface S_k lies between the domains D_{k-1} and D_k . In other words, if we consider a tiling t , and if we particularize the de Bruijn surfaces of the family F_a (see figures 1 and 2), tiles not belonging to the surfaces of F_a are distributed between the different domains.

Now we contract (or delete) the tiles of F_a from the $D+1 \rightarrow d$ tiling t by setting the length of e_a to 0, thus obtaining a $D \rightarrow d$ tiling \tilde{t} . Two adjacent tiles of \tilde{t} , with one above the other along the direction e_a , are either on the same domain D_k or separated by one (or several) de Bruijn surface of F_a , the tile atop being in the higher domain. This allows to define an order relation, \leq_a , relatively to F_a , between any two adjacent tiles u and v : $u \leq_a v$, means that u is below v along e_a and so that u is either in the same domain as v or in a lower domain. Note that we can recover this order relation between any adjacent tiles by orienting all the faces[‡] of a tiling by e_a : given two adjacent tiles u and v of \tilde{t} , $u \leq_a v$ if when one goes from u to v , the face between u and v is crossed in the positive direction (see figure 7).

Now recall that our aim is to position the de Bruijn surfaces of F_{D+1} on a $D \rightarrow 3$ tiling \tilde{t} . One way to do that, is to associate an integer X_u called part to each tile u of the tiling \tilde{t} : X_u is equal to the index k of the domain D_k the tile u belongs to. For example, one tile with a part equal to 3 is on the third domain, so between the

[‡] In this paper we call face of a tile a $d-1$ -dimensional polyhedron generated by $d-1$ orientation vectors.

second and the third de Bruijn surface of the family F_{D+1} , a tile with a part equal to zero being below the first surface. As we have seen it, these parts have to respect the partial relation order \leq_{D+1} , which for convenience we will simply denote by \leq in the following of this paper. Since all tiles belong to one domain, the parts can vary from 0 to p_{D+1} . To generate all the possible $D+1 \rightarrow 3$ tilings from a $D \rightarrow 3$ one, we have to find all the possibilities of filling the tiles of the latter tiling by parts from 0 to p_{D+1} respecting the partial order between the tiles. This type of problem is called a generalized partition problem of height p_{D+1} on the $D \rightarrow 3$ tiling. A solution of this problem is called a (generalized) partition. In the figure 2, one can see an example of a $4 \rightarrow 2$ tiling coded by a generalized partition on a $3 \rightarrow 2$ tiling. The underlying tiling \tilde{t} is called the *base* tiling of the generalized partition problem.

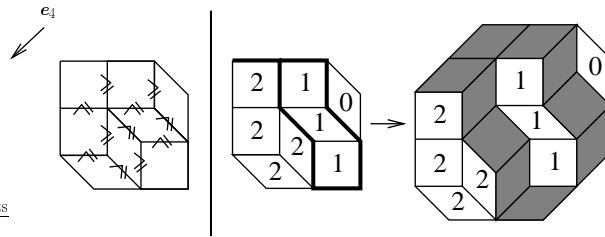


Figure 2. Example of generation of a $4 \rightarrow 2$ tiling by the generalized partition method. Left: Order relation between the tiles of a base $3 \rightarrow 2$ tiling \tilde{t} . Right: one solution of this generalized partition problem codes a $4 \rightarrow 2$ tiling. The tiles of the de Bruijn family F_4 are shaded. The remaining ones belong to the base tiling \tilde{t} . The domains D_0 , D_1 and D_2 appear as the tiles bearing parts equal to 0, 1 and 2 respectively. They are separated by the two de Bruijn surfaces of the family F_4 . From reference [16].

The simplest case is a solid partition problem [15] that is to say a partition problem on a 3-dimensional rectangular array, and therefore on a $3 \rightarrow 3$ tiling. A solid partition problem codes $4 \rightarrow 3$ tilings of codimension 1. Actually to code all the $D+1 \rightarrow 3$ tilings, we have to solve all the generalized partition problems on all the $D \rightarrow 3$ base tilings. Therefore, we have obtained a coding of $D \rightarrow 3$ tilings by successive generalized partition problems.

To sum up, there is a one-to-one correspondence between $D+1 \rightarrow 3$ tilings and pairs composed of a base $D \rightarrow 3$ tiling together with a generalized partition on this base tiling. This one-to-one coding of zonotopal tilings is described in a more formal way in references [7, 16]. It can be naturally extended to any $D \rightarrow d$ tiling problem.

To close this section, let us remark that when one codes $D+1 \rightarrow 3$ tilings by the generalized partition technique, the order in which the de Bruijn families of surfaces are successively added to the tilings is arbitrary. For sake of convenience, one is for example free to choose the D first edge orientations defining the base tilings among the $D+1$ possible ones. Of course, the set of base tilings depend on this choice (see figure 5).

2.3. Definition of cycles

We can now define what we call a *cycle* on a base tiling [16]. If we denote by X_i the part on the tile i , a cycle will be a succession of pairwise adjacent tiles, T_1, T_2, \dots, T_n , such that: $X_1 \geq X_2 \geq \dots \geq X_n \geq X_1$ with respect to the previous order relation on tiles, as

it is illustrated in figure 7. That means that the parts of the tiles inside the cycle have to be equal to a unique part X_0 and have a collective behavior. In particular, their values cannot but change simultaneously. Such cycles are known to exist on specific *ad hoc* $6 \rightarrow 3$ examples. The first one can be found in reference [30] (example 10.4.1) and the second one in [31] (example 3.5), in the context of “oriented matroid theory”. Nothing prevents *a priori* the occurrence of several independent cycles in a same base tiling (possibly bearing different parts). Our forthcoming numerical exploration shows it is actually possible.

One of our purposes is to analyze occurrence of cycles in a more systematic way. In particular, we show that cycles already appear in some $5 \rightarrow 3$ tilings (used to encode $6 \rightarrow 3$ icosahedral tilings by the generalized partition technique). In addition, in the following of this article, we will discuss the possible influence of these cycles on flip dynamics and on the configuration spaces of tilings. Let us emphasize that this problem is specific to dimensions 3 and above, since we shall see that there cannot exist cycles in dimension 2. Before discussing in further details the consequences of these cycles, we now describe what a flip is in a rhombus tiling, and how it is seen in the generalized partition point of view.

3. Basics of flip dynamics and cycles

One can define in rhombus tilings local degrees of freedom which are called elementary flips or localized phasons. In dimension d , a flip consists of a local rearrangement of $d+1$ tiles in a small zonotope inside the tiling. In dimension 2 it is a rearrangement of 3 tiles inside a hexagon, and in dimension 3 of 4 tiles inside a rhombic dodecahedron, see figures 3 and 4. One can already mention that in dimension 2 the configuration space of tilings is proven to be connected *via* these elementary flips (see section 5). Which means that we can go from any tiling to any other one by a finite sequence of flips. In dimension 3, it is an open question that we will address in this paper.

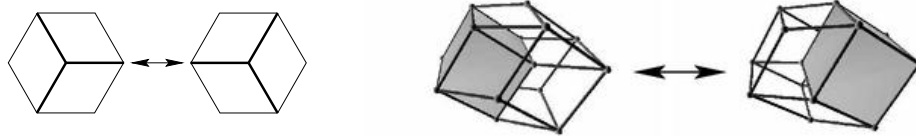


Figure 3. A 2-dimensional flip inside a (not necessarily regular) hexagon involves 3 tiles, and a 3-dimensional flip inside a rhombic dodecahedron involves 4 tiles.

Flips allow to define a Monte Carlo Markovian dynamics on tiling sets as follows [19, 32]: pick up a tiling vertex at random with uniform probability. If this vertex is flippable (it is surrounded by $d+1$ tiles in dimension d), then flip it. This Markovian process converges towards the uniform distribution on the set of tilings provided the configuration space is connected by flips. Note that temperature can be introduced in this point of view to take into account possible interactions between

tiles; the transition rates must be adapted consequently. In this paper, we focus on the infinite temperature limit, where all the configurations have equal equilibrium probability and where all rates of allowed transitions are equal.

This Markovian dynamics has been mainly studied in dimension 2. It has been demonstrated that it is rapid in codimensions 1 [33] and 2 [26]. This means that the typical times to reach equilibrium are polynomial in the system size. The same kind of result has also been established numerically in the $4 \rightarrow 3$ case [10]. In addition, there exist studies concerning diffusion in random tilings evolving *via* this Markovian dynamics. This last point will be discussed in great detail in section 6.

Now, let us see how these flips are seen in the generalized partition point of view. On a generalized partition problem on a $D \rightarrow d$ tiling, which codes a $D+1 \rightarrow d$ tiling, flips can be classified into two types (see figures 4 and 5), following reference [16].

Type-I flips involve only tiles of the base $D \rightarrow d$ tiling and no tile of the de Bruijn family F_{D+1} . As a consequence, the $d+1$ tiles bear equal parts, and these flips only change the base tiling without modifying the parts of the tiles. Type-II flips involve tiles belonging to the de Bruijn family F_{D+1} . More precisely, they involve d tiles having an edge oriented by e_{D+1} , locally representing a surface of the family F_{D+1} , and one tile u of the base tiling. The flip consists in modifying the position of the latter surface with respect to the tile u . So it changes the part X_u borne by the tile u by ± 1 . Regarding one realization of a generalized partition, this flip will be possible if one can modify the part on this tile respecting the partial order on tiles. It will be possible only for tiles at the boundary of zones with two different part values.

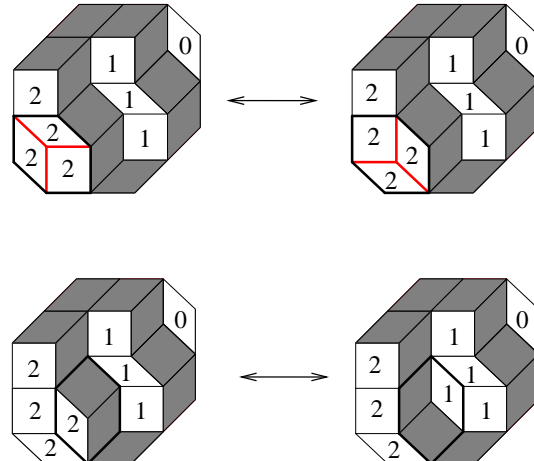


Figure 4. The two types of flips on the $4 \rightarrow 2$ tiling of figure 2. Upper panel: type-I flip involving 3 tiles none of them in the family F_4 . It only affects the base tiling but not the parts it bears. Lower panel: type-II flip involving 2 tiles of the family F_4 and one single tile u of the base tiling. It changes the part X_u borne by u by ± 1 .

One can now build a schematic picture of the configuration space of tilings [16] (see figure 5). Considering $D+1 \rightarrow d$ tilings, one can split up the configuration space into disjoint *fibers*. A fiber contains all the tilings generated by the same generalized partition problem, that is to say which have the same base tiling, see figure 5 for a $4 \rightarrow 2$ tiling example. Type-II flips keep the base tiling and therefore the fiber unchanged, whereas type-I flips change the base tiling and therefore the fiber.

Using this picture, one can show the connectivity of 2-dimensional tiling by flips [16]. Indeed, without cycles in the generalized partitions, we can change the parts on a tile one by one, which make fibers connected by flip of the second type. This point is rigorously established in Appendix B. This connectivity of fibers allows one to put all the tiles of the $D \rightarrow d$ tiling to the same part, releasing all type-I flips on the base tiling. Building our $D+1 \rightarrow d$ tilings on a connected configuration space of base $D \rightarrow d$ tilings, this shows inductively the connectivity of the whole configuration space, starting from the unique $d \rightarrow d$ base tiling. For short, we can say that *if fibers are all connected and if the base is connected itself, then the configuration space is connected in its turn*.

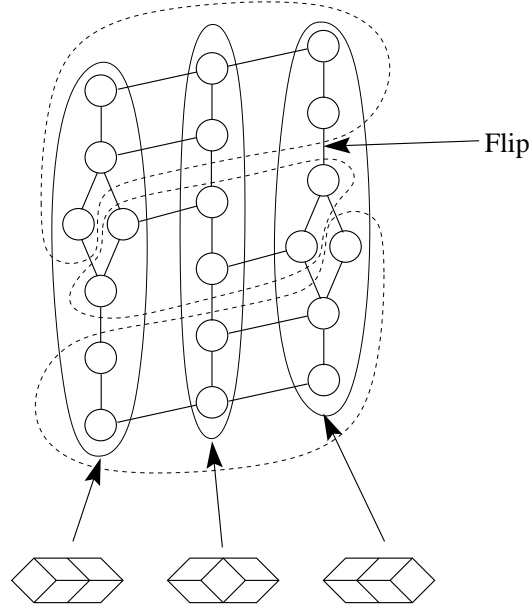


Figure 5. Configuration space of $4 \rightarrow 2$ tilings of an octagon of sides $(2,1,1,1)$. There are 20 tilings represented by vertices. Tilings are linked by an edge if they differ by a single flip. In the generalized partition formalism, the 20 tilings can be distributed among 3 fibers according to their base tiling. The 3 possible $3 \rightarrow 2$ base tilings are represented in the figure. One can see type-I (inter-fiber) flips and type-II (intra-fibers) flips. If one particularizes a different edge orientations from the forth family of lines, the fibration is different. There are 4 different fibrations corresponding to the 4 edges e_a . We have represented two of them (fibers drawn in full and dotted lines, respectively).

Now, we precise the role of the cycles in this picture, and their possible influence on flip dynamics, since we know that they can appear in 3-dimensional tilings. First, we present a cycle example in a $6 \rightarrow 3$ tiling, see figure 7. As we said it previously, a cycle

in a tiling is a sequence of pairwise adjacent tiles that are geometrically constrained to bear the same part in the generalized partition problem. In term of flips, since all parts of the cycle are forced to be equal, the tiles of a cycle cannot participate to a type-II flip which would change the part of a *single* tile to a value different from that of the whole cycle. A direct consequence is that a fiber based on a tiling with cycles cannot be connected anymore by single flips, and the proof for the 2-dimensional connectivity cannot be extended to the 3-dimensional case, except if we are able to prove that there are no cycles in all base tilings. We must also modify our schematic picture of the configuration space when it is based on tilings with cycles, see figure 6. We now have connected fibers based on tilings without cycle, as well as disconnected fibers based on tilings with cycles.

Note that such fibers should be typically a lot smaller than fibers without cycles because of the following heuristic argument. The entropy of a fiber is the number of solutions of a generalized partition problem with N parts, which should grow like $S_0 N$ with S_0 a typical entropy per part. We postulate this behavior because we know the entropy is of this form in codimension-one problems based on (hyper)-solid partition problems [15]. Now a partition problem with cycles can be seen as a partition problem without cycles if one identifies parts of a same cycle. Its entropy is now of order $S_0 N_{eff}$, with N_{eff} an effective number of independent parts. An effective number of parts means the number of tiles which can have a different part. Which makes the entropy of fibers based on tiling with cycles much smaller than the others.

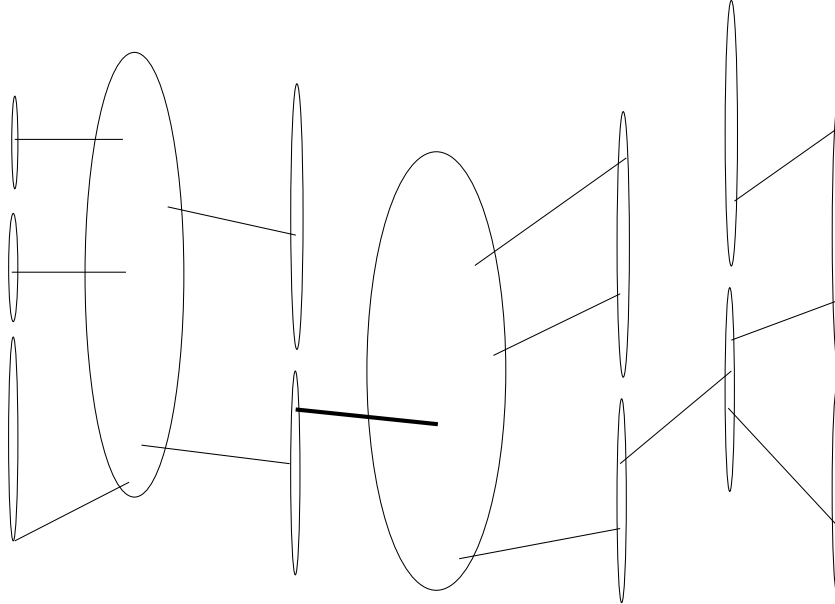


Figure 6. Schematic picture of a configuration space where fibers can be disconnected because of the possible occurrence of cycles. Some fibers are connected if they are associated with base tilings without cycles, some are not. Connected fibers are expected to be bigger than disconnected ones. This configuration space is more intricate than the one of figure 5 and its overall connectivity is not acquired any longer. In particular in this figure, if the flip represented by the thick line is suppressed, the connectivity fails, the space is split into two components.

Geometrically speaking, a cycle is a sequence of tiles making a loop such that each tile is placed above the preceding one relatively to the orientation prescribed by e_{D+1} . In the example of figure 7 this vector is placed perpendicularly to the picture plane. This cycle can be seen analogously to a loop of coins, each one placed above the preceding one. A visible consequence is that we cannot place a de Bruijn surface oriented by the vector e_{D+1} between the tiles of the cycle, as well as we cannot place a horizontal sheet of paper between the coins, splitting the loop between coins above the sheet and below the sheet. Which is equivalent to say that the tiles must bear equal parts.

Let us anticipate on the following to emphasize that these cycles should have an influence not only on the connectivity but also on the Markovian flip dynamics. Indeed they forbid some type-II flips, they reduce locally the degrees of freedom related to those flips. They are susceptible to slow down the dynamics, in the sense of an increase of ergodic times. In the schematic picture of figure 6, one can see that the cycles make the configuration space more intricate. One can imagine that they could create inhomogeneities in the distribution of flip paths through the phase space resulting in entropic barriers. More precisely, in [26], the demonstration of short ergodic times in dimension 2, was based on short ergodic times inside the fibers, which is not possible anymore in presence of cycles. Therefore, one can wonder whether the features of the dynamics are modified by those cycles. It will be the purpose of section 6.

4. Edge orientations, line arrangements and boundaries

Before tackling the questions of connectivity and vertex diffusion, this technical section clarifies the question of non-equivalent edge orientations in 3-dimensional tiling problems and their relation with zonotopal boundaries. Indeed, it will appear in the following that the existence (or not) of cycles in base tilings is closely related to the choice of edge orientations. In particular, we shall be able to prove connectivity by flips for a large majority of edge orientations, but the proof will fail in some minority cases. The classification of edge orientations will be related to a classification of line arrangements in the projective plane \mathbb{PR}^2 .

4.1. Edge orientations and equivalence relation

Random tilings model studies concern the way of arranging simple geometrical structures (the tiles) in the space or in the plane. One possible interest is the contribution to the entropy of such possible configurations. Here we are interested in the way the system can go from one of those configurations to another. The geometry of the tiles does not concern directly those features but rather the symmetries. Indeed, one can imagine to start with a tiling and begin to perturb one orientation of one family of edges. That will deform globally the tiling, but not its topological structure in terms of relative positions of the tiles. More precisely, tile edges can be rotated or elongated provided a modified edge does not cross a plane made to by two other edges, which means there exist no flat tiles and no tiles are overlapping. Which means that the combinatorial properties will remain the same, there exists a one-to-one correspondence between the tiles of the initial tiling and the modified ones.

Given two families of D edges, denoted by $f = (e_1, \dots, e_D)$ and $f' = (e'_1, \dots, e'_D)$, we define them as *equivalent* [34] if one can transform f into f' by the composition of the three following transformations: (i) permutation of the indices; (ii) sign

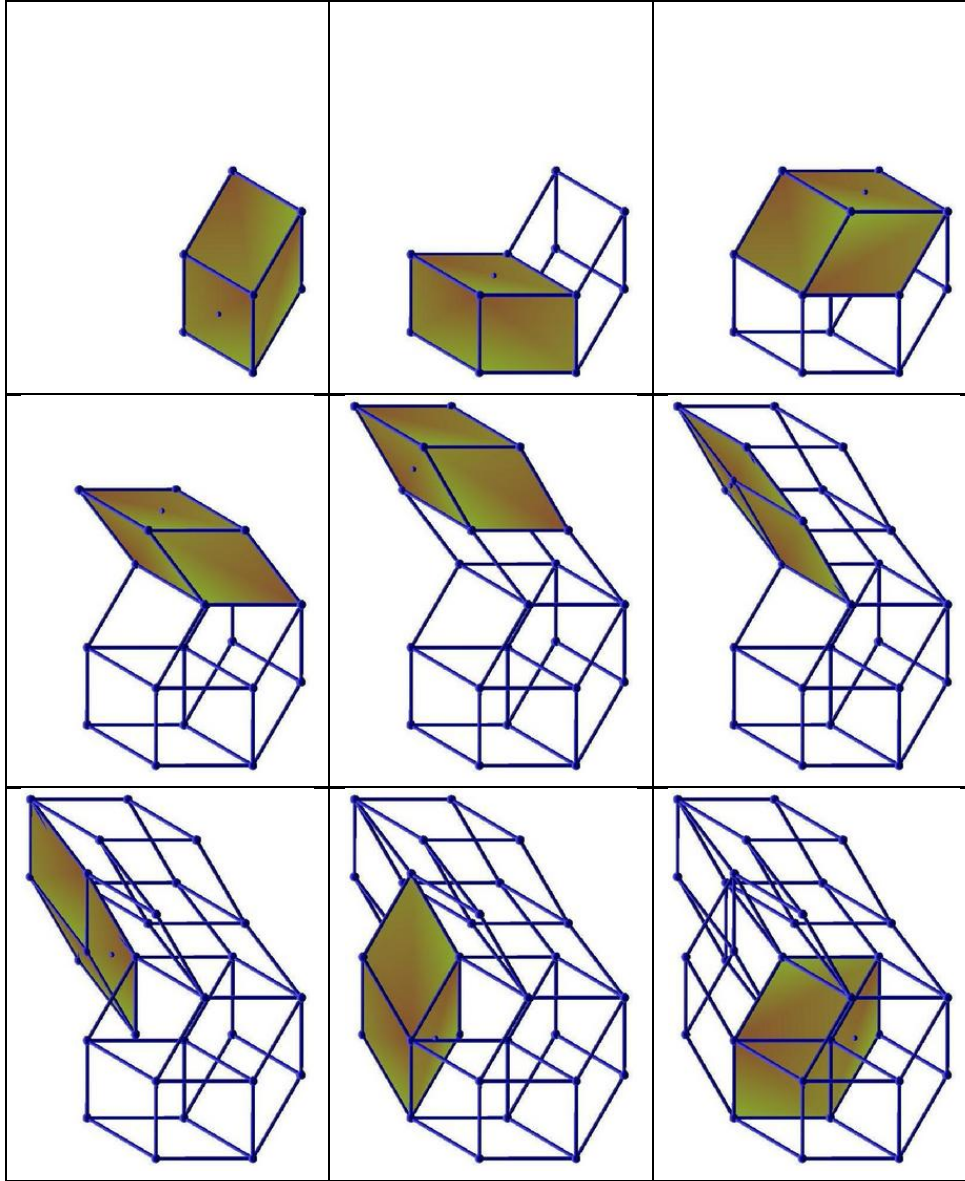


Figure 7. Example of 9-tile cycle in a base unitary $6 \rightarrow 3$ tiling with one de Bruijn surface in each family. We have only drawn the 9 tiles belonging to the cycle whereas the tiling contains 20 tiles. Such cycles already exist in $5 \rightarrow 3$ tilings but the examples we know contain more tiles than the present one. The tiles are added to the cycle one by one. The edge orientation e_7 which orients the tiling is perpendicular to the picture plane and points upwards. As a consequence, given two adjacent tiles t_1 and t_2 separated by a tiling face, t_1 is just above t_2 with respect to the order relation between tiles if t_1 is above t_2 in the figure, in other words if t_1 hides partially t_2 (the face of t_1 that will be covered by t_2 is marked by a dot). Each tile of the cycle is above the preceding one and the last tile is below the first one, which loops the cycle. Note that *this* cycle can be broken by flipping the 4 bottom tiles that form a rhombic dodecahedron.

reversals; (iii) continuous deformation of the vectors \mathbf{e}_a without creating degenerate configurations of three vectors: $\det(\mathbf{e}_{a_1}, \mathbf{e}_{a_2}, \mathbf{e}_{a_3}) \neq 0$ for all (a_1, a_2, a_3) . When the families f and f' are equivalent, we say that they define equivalent sets of rhombic tiles.

To exemplify this notion, we now illustrate that all 2-dimensional sets of tiles are equivalent with respect to this definition. In 2 dimensions, the only way to choose the D edge orientations is on a star configuration, see figure 8. Indeed, imagine again that you have a 2-dimensional set of 3 edges, number them, and then modify the orientation of the third one until it lies between the first and the second one. One can see that the third one plays the same role as the second one before the transformation. By transposing the numbering of these two edges we get an equivalent set of edges. One can see in figure 8 the continuous passage from one set to the other one in a $3 \rightarrow 2$ tiling. By modifying the orientation of the third edge until it lies between the first and the second edge, we obtain an overlapping tiling. To recover the initial tiling we have to transpose the role of the edges 2 and 3 and to place the tiles as in the initial tiling. One can easily see that we can do this process whatever the set of edges we have. What makes the 2-dimensional set of edges unique, is that we cannot particularize an edge, each one plays the same role with respect to the others. We shall see that in three dimensions, the situation is quite more difficult, since there exist non-equivalent families of edge orientations starting from $D = 6$.

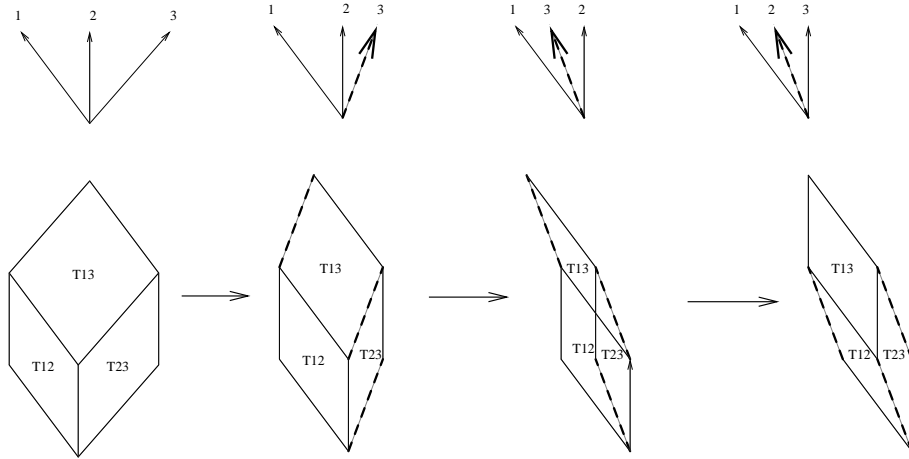


Figure 8. Equivalent 3-edge orientation arrangements in dimension 2 with one of their corresponding unitary tilings. Successive figures from left to right describe the different transformations on these arrangements which let them equivalent. They also represent the results of these transformations on the unitary tilings.

4.2. Line arrangements

To distinguish and enumerate the non-equivalent families of edge orientations, we map families of edges on line arrangements in the projective plane \mathbb{PR}^2 (see [34] for more details). We proceed as follows. The set of edges are represented by a family of D vectors $(\mathbf{e}_1, \dots, \mathbf{e}_D)$. Recall that the signs of those vectors are irrelevant. Those families of vector arrangements are in bijection with arrangements of planes

$(\mathcal{H}_1, \mathcal{H}_2, \dots, \mathcal{H}_D)$, such that for all a , \mathbf{e}_a is orthogonal to \mathcal{H}_a and each \mathcal{H}_a contains the origin. For one given arrangement, since all the planes pass through a common point (*i.e.* the origin), one can get all the information on it by its trace on the projective plane \mathbb{PR}^2 (which is conveniently represented by an affine plane that does not contain the origin. Then this trace is made of lines $(\mathcal{L}_1, \mathcal{L}_2, \dots, \mathcal{L}_D)$ defined as the intersections of the projective plane and the \mathcal{H}_a). So, one can differentiate vector arrangements by differentiating the line arrangements in the projective plane.

We precise now in the line arrangement point of view what equivalent families of edge orientations become. We saw that modifying the orientation of one edge without crossing a plane made by two other edges do not change the equivalence class of a set. In the line arrangement point of view, it corresponds to translate or rotate a given line without crossing an intersection made by two other lines. If three lines intersect in a same point, it means that in the original 3-dimensional space, the three corresponding planes $\mathcal{H}_a, \mathcal{H}_b, \mathcal{H}_c$ contain a common straight line and therefore that the three vectors $\mathbf{e}_a, \mathbf{e}_b, \mathbf{e}_c$ are coplanar. Two line arrangements with D indexed lines will be equivalent if they only differ by a re-indexation of the lines and continuous geometric transformations on the lines which do not create triple points. The equivalence classes of line arrangements in the projective plane, from 4 to 7 lines, are given in the book of Grünbaum [35], see figure 9. We use in the following the indexation of line arrangements of this figure 9. One can see that there exists only one arrangement of four and five lines, whereas there exist four arrangements of six lines and eleven arrangements of seven lines, which correspond to as many different $4 \rightarrow 3$, $5 \rightarrow 3$, $6 \rightarrow 3$, and $7 \rightarrow 3$ random tiling problems. The icosahedral symmetry belongs to the equivalence class of the first arrangement of six lines.

4.3. Polyhedral boundaries

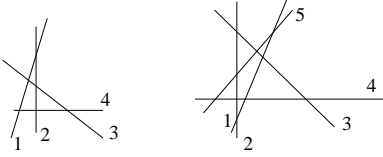
In the following, we study the presence of cycles in tilings associated with all those line arrangements. But let us first discuss how those line arrangements are related to the boundary of the tilings we are considering.

When one applies de Bruijn duality, the boundary of the tiling generated by the partition-on-tiling method is the boundary of the Minkowski sum of the vectors \mathbf{e}_a :

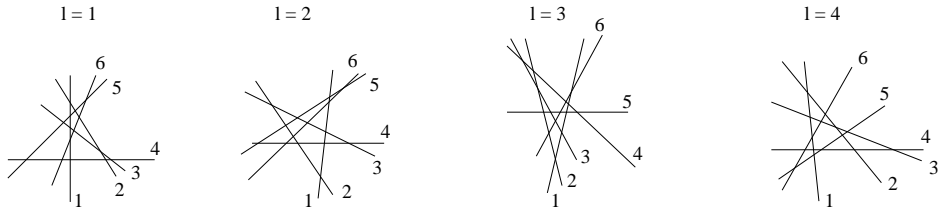
$$Z = \left\{ \sum_{a=1}^D \alpha_a \mathbf{e}_a, \alpha_a \in \mathbb{R}, 0 \leq \alpha_a \leq p_a \right\}, \quad (1)$$

which is also called the *zonotope* generated by the vectors $(\mathbf{e}_1, \mathbf{e}_2, \dots, \mathbf{e}_D)$ [18, 15] (in dimension 2, this zonotope is always a $2D$ -gon of sides (p_1, \dots, p_D) , which is reminiscent of the uniqueness of edge orientations). Zonotopes are convex and centro-symmetric. This boundary is uniquely determined by the choice of the edge configurations, and thus by the choice of the line arrangement in dimension 3. One can directly see this line arrangement by seeing one hemisphere of the boundary of a unitary tiling projected on a plane. The corresponding line arrangement is made by the line crossing each family of edges. These lines are not straight but they can be stretched without changing the crossing topology, see figure 10. Indeed these line arrangements can also be seen as the trace of the dual de Bruijn grid on the projective plane. By definition, the boundary does not depend on the tiling inside this boundary. The line arrangement corresponding to the boundary can always be seen as the trace of the dual de Bruijn grid made by flat de Bruijn surfaces, which always represents a possible tiling. On the figure 10, one can see two tiling boundaries corresponding

Four and five line arrangements:



Six line arrangements:



Seven line arrangements:

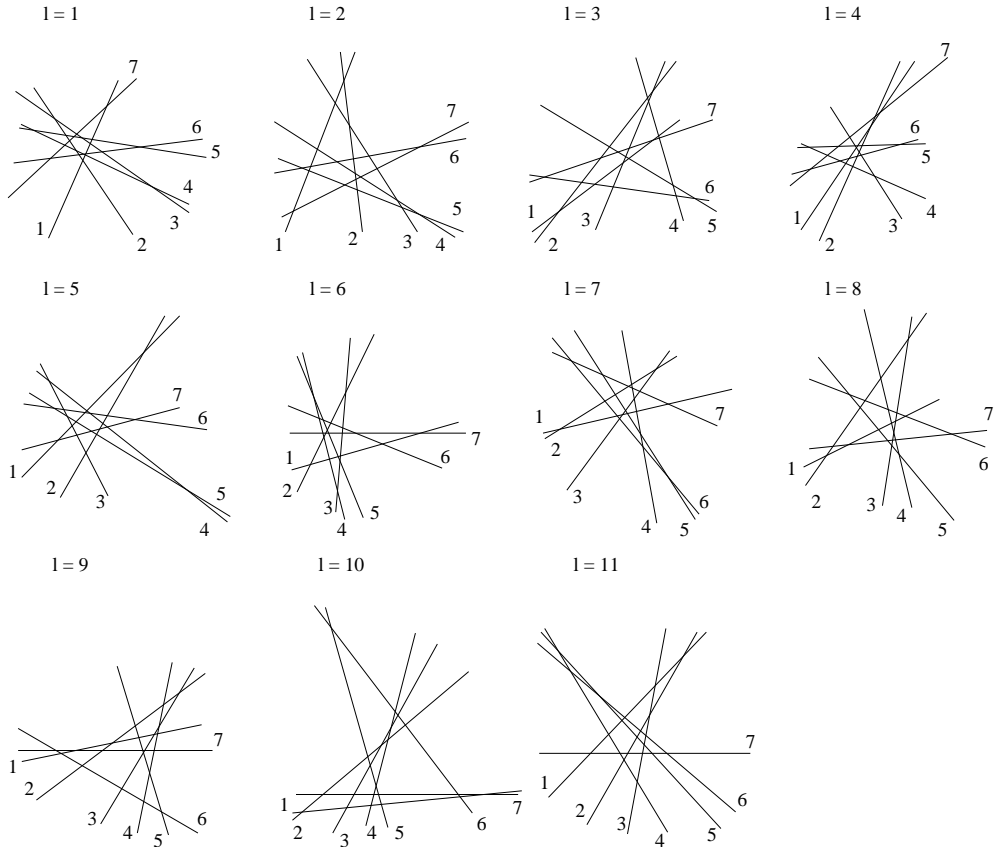


Figure 9. Equivalence classes of line arrangements in the projective plane, from reference [35]. These line arrangements are put in the text in bijection with edge orientations and three-dimensional zonotopal boundaries. There are respectively 1, 1, 4 and 11 arrangements of 4, 5, 6 and 7 lines. The first arrangement of six lines corresponds to the icosahedral symmetry.

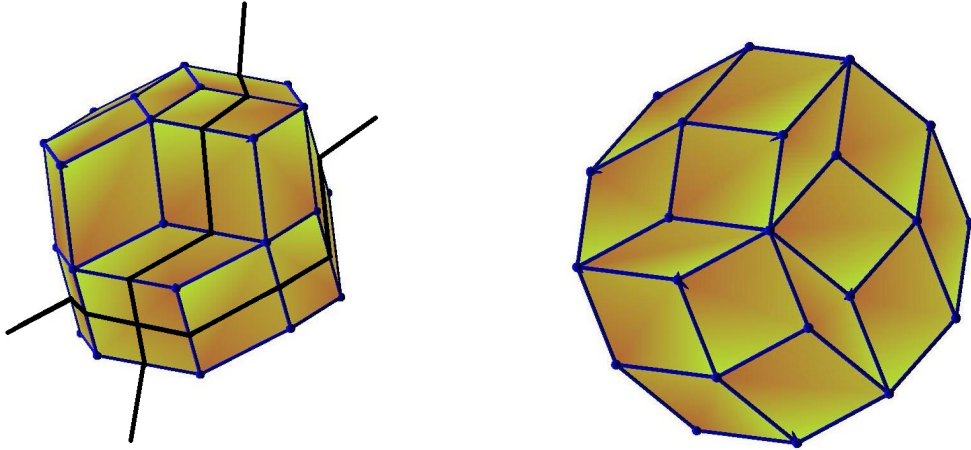


Figure 10. Two topologically different boundaries of (unitary) $6 \rightarrow 3$ tilings. The one on the left corresponds to the icosahedral symmetry and the one on the right to the fourth arrangement of six lines. On the left one, we have represented the trace of two de Bruijn surfaces on the boundary by two black lines. By drawing the lines corresponding to all the de Bruijn surfaces on this boundary, one builds an arrangement of lines which can be stretched and one obtains the first 6-line arrangement. A visible difference between these two boundaries is the connectivity of each vertex. On the right boundary there exists a vertex with six edges which is absent on the left one. This vertex of connectivity six is represented by an irregular hexagon in the fourth 6-line arrangement.

to the icosahedral tiling and to the fourth line arrangement with six lines. One can remark that two-line intersections correspond to faces of the boundary. In particular these two boundaries differ by the existence of a vertex of connectivity six in one of the two boundaries. This is seen in the fourth line arrangement by the presence of one hexagon. By contrast, the total number of tiles N_T does not depend on the choice of the boundary because the de Bruijn grid is complete:

$$N_T = \sum_{a < b < c} p_a p_b p_c. \quad (2)$$

To characterize the differences between random tilings with non-equivalent edge orientations, we have enumerated tilings with unitary boundaries (*i.e.* with one de Bruijn surface per family), see tables 1 and 2. For unitary tilings it is possible to span all the configuration space for each boundary condition. Indeed, we demonstrate in the following that the configuration space of all the random tilings with unitary boundaries are connected for codimensions up to 4 which are under interest in the present paper. These results, which are exact, show definitively that tiling problems with non-equivalent families of edge orientations cannot be put in one-to-one correspondence since they do not have the same number of configurations. There are 160 unitary tilings built on the first 6-line arrangement, that is to say with icosahedral symmetry.

In the next section we propose a demonstration of the connectivity for most boundaries, based on an analysis of the corresponding line arrangements in the aim of predicting the occurrence of cycles.

Unitary $6 \rightarrow 3$ tiling space				
Line arrangement	1	2	3	4
# Tilings	160	148	144	148

Table 1. Number of tilings in the configuration spaces of unitary $6 \rightarrow 3$ tilings as a function of the line arrangement. These results have been computed by entirely spanning the configuration space numerically.

Unitary $7 \rightarrow 3$ tiling space											
Line arrangement	1	2	3	4	5	6	7	8	9	10	11
# Tilings	7686	8260	7624	7468	7220	7690	7518	7242	7106	6932	6902

Table 2. Number of tilings in the configuration spaces of unitary $7 \rightarrow 3$ tilings as a function of the line arrangement.

5. Connectivity and structure of the configuration space

5.1. Connectivity

Before presenting the principles of the proof of connectivity and applying them to dimensions 2 and 3, we provide the broad outline of this technical subsection.

A family of D indices (q_a) is attached to each tile u of a base $D \rightarrow d$ tiling \tilde{t} . For each family of de Bruijn surfaces F_a , if u belongs to a surface S_k of F_a , then the index $q_a(u)$ is equal to k . If u lies between the surfaces S_k and S_{k+1} , in the domain D_k , then $q_a(u)$ is half-integer and is equal to $k + 1/2$.

We prove that under favorable conditions, more precisely *if e_a and e_{D+1} are “companion” vectors in the family of edge orientations* as defined below, then the function $u \mapsto q_a(u)$ is monotonous with respect to the order relation between tiles induced by e_{D+1} .

As a consequence, q_a cannot but be constant along a cycle. Therefore the cycle either lies entirely in a single de Bruijn surface of F_a or strictly lies between two of them. In the first case, the cycle lives in the equivalent of a $D - 1 \rightarrow d - 1$ tiling, and in the second case in a $D - 1 \rightarrow d$ tiling. If we can prove inductively that cycles cannot exist in such tilings, we get that they cannot exist in $D \rightarrow d$ tilings under interest.

5.1.1. Principles of the proof

We have seen in section 3 that the connectivity of the configuration space by elementary flips can be demonstrated for particular tiling problems using the partition-on-tiling method. These particular tiling problems are those for which all fibers are connected, which means that the underlying base tilings do not contain cycles. We recall that the proof is based on an induction: supposing that the space of base tilings is connected, the whole connectivity relies on the connectivity of all fibers.

When one codes tilings by the generalized partition technique, there are $D + 1$ ways to choose the direction e_{D+1} among edge directions. For example, in order to build a $5 \rightarrow 3$ tiling, we begin with a $3 \rightarrow 3$ tiling, but we have to choose with which of the five final edge orientations we build this tiling, we have $\binom{5}{3}$ possibilities. To extend a base $3 \rightarrow 3$ tiling to any $4 \rightarrow 3$ one by filling the partition, we also have to choose which is the fourth edge and finally which is the fifth edge in the $5 \rightarrow 3$ tiling. As a consequence, there are $D + 1$ different decompositions of the configuration space into

fibers. We say that there are $D + 1$ different fibrations. We insist again on this point because in order to demonstrate connectivity, it is sufficient to exhibit one fibration among the $D + 1$ possible ones, the fibers of which are connected.

In terms of line arrangements, it means that given an arrangement of $D + 1$ lines, we have to particularize one line, such that D lines correspond to edge orientations of the $D \rightarrow 3$ base tilings, whereas the $(D + 1)^{th}$ one orients these base tilings. We now show how one can demonstrate that for some line arrangements with one line particularized, they cannot correspond to partition-on-tiling with cycles, which demonstrates the connectivity of the corresponding random tiling space. To begin with, we explain the principle of the demonstration in dimension d , use it to prove that there cannot exist cycles in any tiling of dimension 2, and finally to treat most cases of dimension 3.

We first have to consider that a cycle is a succession of pairwise adjacent tiles, sharing faces, that form a closed, oriented path in the tiling. To characterize this path, we have to be able to precise the position of any tile in this tiling, which is entirely determined by D numbers as follows.

We position the tiles with respect to the de Bruijn surfaces of the D families. As we saw it previously, de Bruijn surfaces of each family divide the space \mathbb{R}^d in disjoint domains. One can completely characterize the position of a tile in the whole tiling by assigning to which domains it belongs and which de Bruijn surfaces intersect the tile. For that, we introduce D indices q_a , $a = 1, \dots, D$, attached to each tile. d of the q_a are integers and characterize de Bruijn surfaces which intersect the tile, and $D - d$ are half-integers giving the domains, defined by the family surfaces which do not intersect the tile, where the tile is. For example, an index $q_3 = 2.5$, corresponds to a tile which is between the second and the third surfaces of the third family. Let us remark, that when we code a $D + 1 \rightarrow d$ tiling, t , by a generalized partition on a $D \rightarrow d$ tiling, \tilde{t} , the parts X_u on each tile of \tilde{t} correspond to the domain, defined by the $(D + 1)^{th}$ family surfaces, they belong to. For the tiles u of \tilde{t} in t , we have $q_{D+1} = X_u + 0.5$.

Now, since a cycle is a closed path between the tiles, for each indices q_a we have $\Delta q_a = 0$ along the cycle. Which means that if it exists a positive Δq_a between two adjacent tiles of the cycle, it must exist some negative Δq_a between some other adjacent tiles of the cycle. To prove that there cannot exist cycles in some tiling, we prove that for some families F_a , Δq_a is always positive (or always negative) along an oriented path between the tiles.

More precisely, each q_a defines a function on the partially ordered set of the tiles. We say that for some family F_a , q_a is *monotonous* if given any two tiles u and v , if $u \geq v$ then $q_a(u) \geq q_a(v)$. Note that we can in a similar way define the notion of *monotonously decreasing* q_a , which is equivalent to the previous one up to a sign reversal of e_a .

But, by definition, the tiles of a cycle (u_1, \dots, u_n) are such that: $u_1 \geq u_2 \dots \geq u_1$, where u_i, u_{i+1} are adjacent tiles, which means that $u_1 = u_2 = \dots = u_n$. So if for a family F_a , q_a is monotonous, then the tiles of a cycle have to be at a constant q_a . In other words, the cycle lives either on a de Bruijn surface of the family F_a (if q_a is an integer), either in one of the domains defined by the surfaces of this family (if q_a is half-integer). In the first case, the cycle has to live in the equivalent of a $D - 1 \rightarrow d - 1$ tiling (see section 2.1). In the second case, it has to live in a $D - 1 \rightarrow d$ sub-tiling. To prove that there cannot exist cycles for the tiling made by a family of D edge orientations f , we proceed by induction. We prove that for a family F_a , q_a is monotonous for any tiling based on f . Then we prove that there cannot exist cycles

in $D-1 \rightarrow d-1$ tilings based on $f - \{\mathbf{e}_a\}$, as well as in $D-1 \rightarrow d$ tilings by repeating the procedure on these tilings. The procedure stops when we have to prove the non-existence of cycles in tilings for which it is already proven, either in $D \rightarrow 1$ tilings, or in $d \rightarrow d$ tilings. Indeed, a cycle cannot exist in a one-dimensional tiling with fixed boundaries where it is impossible to make a closed path of pairwise adjacent tiles. In the $d \rightarrow d$ tiling, which is the periodic one, it is also clear that cycles cannot exist: the partial order between the tiles corresponds to the partial order given by d independent coordinates. Therefore it is impossible to build a cycle in the d -dimensional lattice because the previous coordinates cannot but increase along a cycle.

We show in the following that in dimension 2, it is always possible to find (at least) one family F_a among the D possible ones such that q_a is monotonous. We then show the same in dimension 3 for almost all the families of edge orientations of codimension up to 3.

To prove the monotony for one q_a , on all the tilings based on a family of edge orientations, we prove the monotony for any two adjacent tiles u and v . We have to consider how the indices can change when we go from one tile to another adjacent one. Between two adjacent tiles, only two indices can differ. Indeed, they share one face which corresponds to the intersection of $d-1$ de Bruijn surfaces, and so to $d-1$ integer indices q_a , pairwise equal in each tile. Since they are adjacent, they cannot be separated by a de Bruijn surface. As a consequence, the indices which are half-integers in each tile for a same family have to be equal. It remains only two indices which can differ from one tile to the other. They correspond to the indices of the surfaces which intersect the two adjacent tiles but do not correspond to their shared face. Note that, if the two adjacent tiles are intersected by the surfaces of the same family they differ by only one index q_a such as $q_a(v) - q_a(u) = \pm 1$. Let consider two adjacent tiles u and v which are intersected by the surfaces of indices $(q_{a_1}, \dots, q_{a_d})$ and $(q_{a_1}, \dots, q_{a_{d-1}}, q_{b_d})$ with $a_d \neq b_d$. They share the face \mathcal{F} defined by the intersection of de Bruijn surfaces of the families $F_{a_1}, \dots, F_{a_{d-1}}$. The indices for which they differ are q_{a_d} and q_{b_d} , with $\Delta q_{a_d} = q_{a_d}(v) - q_{a_d}(u) = \pm 0.5$ and $\Delta q_{b_d} = \pm 0.5$, as we explained it above. The sign of each variation depends on the position of each tile with respect to the other one. If to go from u to v we are crossing their common face along the direction \mathbf{e}_{a_d} , then $\Delta q_{a_d} = 0.5$. In other words, one can orient \mathcal{F} by \mathbf{e}_{a_d} and if v rests on the positive side of \mathcal{F} then $\Delta q_{a_d} = 0.5$. The same holds for Δq_{b_d} . Furthermore, if $v \geq u$ with respect to the partial order defined by \mathbf{e}_{D+1} , that means that v rests on the positive side of \mathcal{F} defined by \mathbf{e}_{D+1} . So an index q_a is monotonous for every pair of adjacent tiles, if the orientations made by \mathbf{e}_a , of *all the face species* that do not contain \mathbf{e}_a , are identical to those made by \mathbf{e}_{D+1} .

We call *companion* vectors (in a family of edge orientations f), two vectors \mathbf{e}_a and \mathbf{e}_b which orient equivalently all the faces made by the remaining vectors of $f - \{\mathbf{e}_a, \mathbf{e}_b\}$ (up to a possible sign reversal of \mathbf{e}_a or \mathbf{e}_b). To sum up this subsection, *whenever one identifies a companion vector \mathbf{e}_a of \mathbf{e}_{D+1} , the index q_a is a monotonous function with respect to the partial order relation between the tiles induced by \mathbf{e}_{D+1} .*

We now explicit how to identify companion vectors in the 2-dimensional case, before focusing on the 3-dimensional one.

5.1.2. Dimension 2

We represent families of D edge orientations as in dimension 3. A family of edges is equivalent to an arrangement of vectors in \mathbb{R}^2 , up to sign reversal, which is in turn

equivalent to an arrangement of lines, normal to the previous vectors that all cross at origin. This arrangement of lines can equivalently be viewed on the projective line \mathbb{PR}^1 , where line arrangements are represented by point arrangements, see figure 11. In this representation, it is easy to see that all sets of D edges are equivalent, no particular position can exist. In \mathbb{R}^2 , we represent the $(D+1)^{th}$ orientation vector by a horizontal line. Our aim is to find a companion vector of e_{D+1} among the D possible ones, such that at each time one crosses a face (*i.e.* an edge in dimension 2) following this vector direction we also cross this face in the positive direction defined by e_{D+1} . By representing a line arrangement as well as the corresponding boundary, see figure 11, one can easily see that such vectors exist and are represented by the closest lines to the horizontal one. If we take as the projective line the line parallel to the horizontal one, the $(D+1)^{th}$ vector is represented by the point at infinity, and we prove below that the vectors which fulfill our conditions are represented by the extremal points. Note that the direction chosen to represent the projective line is not relevant, if we take a projective line not parallel to the horizontal one, the $(D+1)^{th}$ vector is represented by a particular point on the line, and the vectors which fill our conditions are now represented by the points nearest to this particular one, as previously where it was at infinity, see figure 11.

More precisely, we present now how we can identify companion vectors of e_{D+1} in a family f of D vectors by analyzing the corresponding arrangements of $D+1$ points on an affine line. One can represent the projective line by the unit 1-sphere S^1 , on which antipodal points are identified, see figure 12. Each edge orientation e_a is represented by two antipodal points, \mathcal{P}_a and \mathcal{P}'_a , which are the trace of the central line arrangement previously defined. These two points separate S^1 into two hemispheres (or half-circles). For each a we choose a positive and a negative hemisphere defined by the corresponding vector e_a : this vector points from the negative to the positive hemisphere. Our aim is to understand how each face species \mathcal{F}_a is oriented by the different vectors e_b , $b \neq a$. We represent the orientation of a face \mathcal{F}_a by a vector e_b , by a unitary vector \mathbf{n}_a^b normal to the face \mathcal{F}_a .

We show that a face \mathcal{F}_a is oriented differently by two vectors e_b and e_c , if its representing point on S^1 lies on opposite sides for e_b and e_c . Consider the point \mathcal{P}_a on S^1 representing the face \mathcal{F}_a . Its position is given by a vector $\mathbf{r}_a \in \mathbb{R}^2$. By definition the direction normal to \mathcal{F}_a lies on the line whose trace on S^1 is \mathcal{P}_a . So a normal vector to \mathcal{F}_a is collinear to \mathbf{r}_a . If \mathcal{P}_a lies on the positive side of a point \mathcal{P}_b then: $\mathbf{r}_a \cdot \mathbf{e}_b > 0$. We also have by definition $\mathbf{n}_a^b \cdot \mathbf{e}_b > 0$ so $\mathbf{n}_a^b = \mathbf{r}_a$. Whereas, if \mathcal{P}_a lies on the negative side of a point \mathcal{P}_c , $\mathbf{r}_a \cdot \mathbf{e}_c < 0$, and so $\mathbf{n}_a^c = -\mathbf{r}_a$. Note that this result does not depend on which antipodal point representing \mathcal{F}_a we are considering. Indeed, for the antipodal point of \mathcal{P}_a , \mathcal{P}'_a , we have $\mathbf{r}'_a = -\mathbf{r}_a$, but $\mathbf{r}'_a \cdot \mathbf{e}_b < 0$ since \mathcal{P}'_a lies on the negative side of \mathcal{P}_b , and so $\mathbf{n}_a^b = -\mathbf{r}'_a = \mathbf{r}_a$. To represent the orientation of each face one can consider only one hemisphere of S^1 . The hemisphere we choose is irrelevant. This hemisphere can be identified to the affine line, to which we add the point at infinity to take into account the point at the equator. Following what we said above, on this line one can identify companion vectors as the points which split the line into two sides equivalent for all the other points (up to a possible sign change of one of the two companions). All the points which lie on the positive side of one companion also all lie on the positive side of the second one (or all lie on its negative side). It is now clear that companion vectors are always represented by adjacent points on the projective line, see figure 11. That is why on the projective line, companion vectors

of e_{D+1} are represented by points adjacent to the one representing e_{D+1} . These two points always exist whatever the family of edge orientations represented on the line.

As we discussed it before, that proves inductively on D that cycles cannot exist on generalized partition based on rhombus tiling of dimension 2 and so the connectivity of such tilings follows. Note that this result was already stated in [30] (proposition 10.5.7) and [31] (corollary 4.5) in the context of oriented matroid theory. We now use similar arguments to analyze the 3-dimensional case, and prove that most of the tilings of co-dimension smaller than 3 cannot possess cycles.

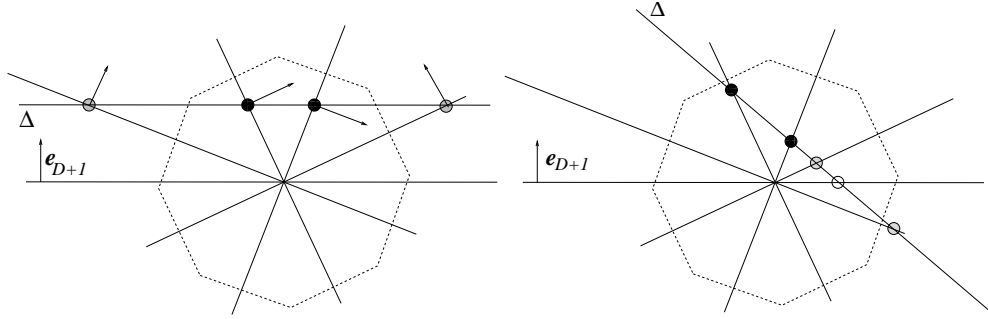


Figure 11. This figure represents 2-dimensional vector arrangements with their representations by central line arrangements and finally by point arrangements on the projective line. It also represents the corresponding boundary of the tiling. The horizontal line represents the vector e_{D+1} which orients the partitions on the tilings. Companion vectors of the latter one are represented on the projective line by gray points which are adjacent to the point representing e_{D+1} (which is the point at infinity in the left figure), whatever the affine line Δ we choose to represent the projective line: a horizontal line on the left figure, and another line on the right one.

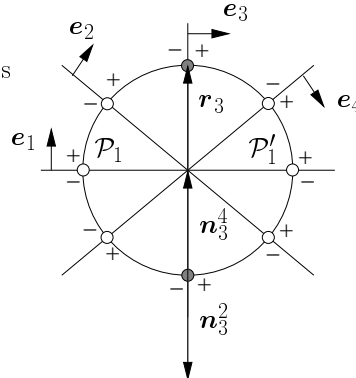


Figure 12. A 2-dimensional vector arrangement and its representation on the 1-sphere S^1 . Each vector, represented by two antipodal points on S^1 , decomposes S^1 into two hemispheres, one positive and one negative. The top gray point representing e_3 , lies both on the positive side of e_2 and on the negative side of e_4 . The orientation of the face \mathcal{F}_3 borne by e_3 is therefore different for these two vectors: $\mathbf{n}_3^2 \neq \mathbf{n}_3^4$.

5.1.3. Dimension 3

Following the previous demonstration, if one finds from a family of D orientation vectors, coding for $D \rightarrow 3$ tilings, one vector \mathbf{e}_a which is companion of \mathbf{e}_{D+1} , cycles can only exist either on the corresponding de Bruijn surfaces of family F_a , or in the tiling of codimension $D - d - 1$ obtained by the contraction of F_a . In dimension 3, the first possibility means to build a cycle on a 2-dimensional surface which we proved to be impossible. So, only the second possibility may exist.

To identify companion vectors from a family we proceed as in dimension 2 to analyze the corresponding line arrangement on the projective plane. We represent the projective plane by the unit 2-sphere S^2 on which antipodal points are identified. The lines on $\mathbb{P}\mathbb{R}^2$ are now represented by great circles on S^2 for which we also define positive and negative sides by the corresponding vectors \mathbf{e}_a . Faces are represented by the intersections of pairs of circles and so by points as in dimension 2.

We now prove that if a point lies on the positive side of two circles the corresponding face is oriented equivalently by the two corresponding vectors. As in the previous section, we precise the orientation by a vector \mathbf{e}_c of a face $\mathcal{F}_{a,b}$ defined by \mathbf{e}_a and \mathbf{e}_b . We assign this orientation by a unitary vector $\mathbf{n}_{a,b}^c$ normal to $\mathcal{F}_{a,b}$. The position of a point $\mathcal{P}_{a,b}$ corresponding to a face $\mathcal{F}_{a,b}$ is given by $\mathbf{r}_{a,b} \in \mathbb{R}^3$. $\mathcal{F}_{a,b}$ is made by two vectors \mathbf{e}_a and \mathbf{e}_b and so $\mathcal{P}_{a,b}$ is the trace on S^2 of the intersection of the planes \mathcal{H}_a and \mathcal{H}_b previously defined. So $\mathbf{r}_{a,b}$ lies on the intersection of \mathcal{H}_a and \mathcal{H}_b and is collinear to any $\mathbf{n}_{a,b}^c$. Now by definition, if $\mathcal{P}_{a,b}$ lies on the positive side of a great circle \mathcal{C}_c corresponding to \mathbf{e}_c , we have: $\mathbf{r}_{a,b} \cdot \mathbf{e}_c > 0$. Since $\mathbf{n}_{a,b}^c \cdot \mathbf{e}_c > 0$, then $\mathbf{n}_{a,b}^c = \mathbf{r}_{a,b}$. On the contrary, if $\mathcal{P}_{a,b}$ lies on the negative side of \mathcal{C}_c , we find that $\mathbf{n}_{a,b}^c = -\mathbf{r}_{a,b}$. As in dimension 2, the same relations hold if we consider the antipodal point corresponding to $\mathcal{F}_{a,b}$. To find companion vectors one can use any hemisphere of S^2 represented by an affine plane to which we add the line at infinity. On this plane, companion vectors are represented by lines \mathcal{L}_c and \mathcal{L}_d such that all the points made by the intersection of two lines different from \mathcal{L}_c and \mathcal{L}_d are on the same sides of \mathcal{L}_c and \mathcal{L}_d , up to a possible sign change of \mathbf{e}_c or \mathbf{e}_d . For an example of an arrangement with companion lines see figure 13.

The previous analysis can be well understood geometrically by considering one arbitrary hemisphere of the boundary of a unitary tiling corresponding to a given arrangement, see figure 13. In this figure, the vector \mathbf{e}_{D+1} is perpendicular to the figure plane. It orients all the faces from bottom to top. Since the boundary is convex, one can easily check that in this representation, a companion \mathbf{e}_a of this vector is such that the arrangement is completely situated on one side of the line \mathcal{L}_a . Whereas a vector \mathbf{e}_b such that the line \mathcal{L}_b divides the arrangement into two non-empty parts cannot be a companion of \mathbf{e}_{D+1} . Indeed, if \mathbf{e}_b orients the faces on the right of \mathcal{L}_b from bottom to top, one can see that it orients the faces on the left of \mathcal{L}_b from top to bottom.

The first arrangement of six lines is an example for which we cannot find any companion lines. That means that we cannot state on the absence of cycles in the generalized partitions based on this arrangement. Actually, we will see in the following that we *do* find cycles on these generalized partitions. In fact, for each arrangements for which we cannot prove the absence of cycles we find them by numerical exploration, see tables 3 and 4, and section 5.2. In these tables, the 0 represents tiling problems for which the analysis of the corresponding line arrangements show that they cannot possess cycles in the corresponding fibration. Note that there exist only three

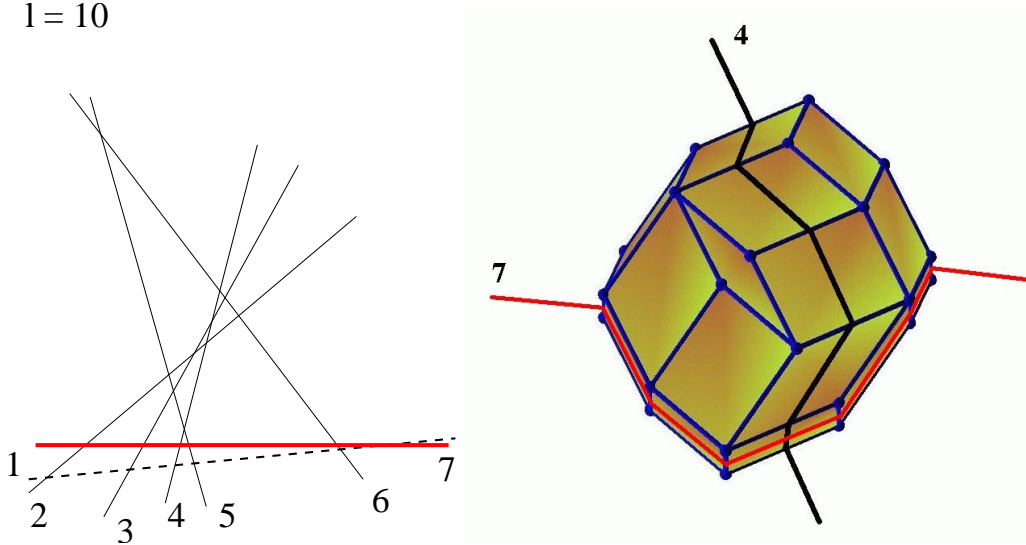


Figure 13. On the left, the tenth 7-line arrangement where we have represented two companion lines, 1 and 7. All the intersections of any two remaining lines are on the same sides of these companion lines. On the right, one possible view of the corresponding boundary of this line arrangement. The vector e_1 (which orients the base tilings in this figure) is perpendicular to the plane of the figure and points upward. The corresponding tiling edges cannot be seen on this figure. But one can easily see that e_7 is companion to e_1 : The trace of the seventh de Bruijn surface is represented on this boundary by the bottom curve. It crosses edges borne by e_7 . One can check that, because of convexity of the zonotopal boundary, the sign of e_7 can be chosen so as to orient all the faces which do not belong to the trace of the seventh de Bruijn surface from bottom to top as e_1 does. On the contrary, the vector e_4 is not companion of e_1 : The trace of the forth de Bruijn surface is represented by a line which splits the boundary into two non-empty parts. If the faces on the left of this line are oriented from bottom to top by e_4 , it will orient the ones on the right from top to bottom.

arrangements (among 17) of at most seven lines for which there is no fibration without cycles. The other arrangements correspond to tiling problems with at least one fibration which is connected. A detailed study of these arrangements also shows that the corresponding base tiling sets are connected. So for all these 14 latter arrangements, we prove the connectivity of the corresponding tiling sets for any tiling size.

By contrast, sets of *unitary* tilings are connected for any codimension lesser than 4. Indeed, we proved by systematic numerical exploration of sets of unitary tilings of codimension lesser than 3 that there always exists a fibration without cycles in this case.

In order to prove the connectivity for the tiling problem for which all fibration exhibit cycles, we would have to prove that one can always break the cycles by type-I flips (see figure 7). Which means that there exists a sequence of flips which brings the tiling from any disconnected fibers to a connected one. Then one can change the parts of the tiles of previous cycles by type II-flips, and bring back the tiling to another component of the initial disconnected fiber. Note that there always exist connected fibers corresponding to the tilings made by flat de Bruijn surfaces as we explain it

below. We have not established a possibility to break those cycles in all cases, and therefore the connectivity problem remains open.

In principle, the arguments developed in this section can be extended to any $D \rightarrow d$ tiling problem using arrangements of hyper-planes in the projective space \mathbb{PR}^{d-1} provided one knows their classification for fixed D and d . In Appendix A, we prove connectivity for codimension 2 tilings of any dimension. Note that independently of this work, and after introducing a new and different formalism, Frédéric Chavanon and Éric Rémila quite recently also established connectivity in codimension 2 [36].

5.2. Abundance of cyclic base tilings ; mean-field argument and numerical studies

We now present numerical results on the abundance of base tilings with cycles (that we also call “cyclic base tilings”) of dimension 3 as a function of their boundary size, as well as a mean-field argument to account for these results. In this section, we focus on diagonal tilings: $p_a = p$ for any a .

We numerically sample the tiling configuration space. We use the Monte Carlo Markovian dynamics described in section 3. The unit of time is set to a number of Monte Carlo steps equal to the number of vertices in the tiling (denoted by N_v) and is called a Monte Carlo sweep (MCS). To get almost independent samples, we wait an equilibration time equal to $p^2 \sim N_v^{2/3}$ between two samples. Indeed, ergodic times in dimension 2 [33, 26] and in $4 \rightarrow 3$ tilings [10] are of this form and we suppose that it is also the case in greater codimension. This is corroborated by our numerical results on diffusion, see the end of section 6.

We start with tilings dual of arrangements of flat de Bruijn surfaces and wait for an equilibration time. Note that these tilings cannot posses cycles. Indeed, in de Bruijn space, tiles are linked by de Bruijn lines which are the intersection of pair of de Bruijn surfaces. The orientation of face species by e_{D+1} in tiling space corresponds to the orientation of these de Bruijn lines by e_{D+1} . In the case of flat de Bruijn surfaces, de Bruijn lines are straight. By following these lines in the positive direction one always heads towards the direction of e_{D+1} , which makes impossible to describe a cycle. We emphasize that in the general case, oriented de Bruijn lines globally point towards e_{D+1} but can locally point in the opposite direction which makes possible the existence of cycles. After each sampling time step, we check whether the tiling possesses a cycle. For unitary tilings, we completely cover the configuration space (by use of a deep search algorithm), therefore the results are exact.

We have made this numerical experiment for all the tiling problems corresponding to 6 and 7-line arrangements, with one particularized line of index λ_{sup} to orient the partitions on tilings. So we checked cycle abundance in all possible $5 \rightarrow 3$ and $6 \rightarrow 3$ base tiling types, coding respectively for $6 \rightarrow 3$ and $7 \rightarrow 3$ tilings. To check if an oriented graph possesses cycles is a complex algorithmic problem, since its complexity grows extremely rapidly with the number of vertices. The complexity of the algorithm we used scales with the number of tiles $N_T = \binom{D}{3}p^3$ as $\ln(N_T)N_T^3$. It is why we have restricted our study to p between 1 to 8 for $5 \rightarrow 3$ tilings and p between 1 to 5 for $6 \rightarrow 3$ tilings. Typically, for $p = 2$ we checked 10^6 independent tilings whereas for $p = 8$ (or $p = 5$ for $6 \rightarrow 3$ tilings) we checked only 500 ones. Typical cycle abundance we found are represented in figure 14. For all the tiling problems for which we prove that cycles cannot exist we effectively never find them. For the other ones, we find cycles and their occurrence increases rapidly with the tiling size p for all cases with a similar law. The differences come from that cycle existence does not arise at the

same size for all those tiling problems. In particular, cycles do not exist in unitary $5 \rightarrow 3$ tilings (exact results) and they appear starting from $p = 2$. For $6 \rightarrow 3$ tilings for which it exists cycles in the unitary case, the cycle fraction is already close to 1 for $p = 5$. These results show that when cycles can exist in a tiling problem, they are certainly very frequent for tilings at large size p . Indeed, if a small cycle appears in a small tiling, it will be likely to appear locally in a large one which can be seen in a first approximation as a juxtaposition of nearly independent smaller tilings.

Following this idea, we now propose a mean-field argument to support these results. For a tiling problem in which cycles are possible, we suppose that there is a non-zero probability α that a tile belongs to a cycle. If all the tiles are considered as independent, the probability that no tile belongs to a cycle in the whole tiling is then $(1 - \alpha)^{N_T}$ and the fraction of cyclic tilings reads:

$$1 - (1 - \alpha)^{N_T}. \quad (3)$$

This supposes that α is independent of the tiling size. It is necessarily false since we have seen that in some cases cycles appear only starting from a given size. But one can think that it is a good approximation for large sizes. The fits of the measured fraction of cyclic tilings by this simple law reproduce well the results in all the cases, see figure 14. A summary of these fits is given in tables 3 and 4. We mention that tiling problems based on the same line arrangement but with a different particularized line λ_{sup} are not necessarily different. In particular, the 6 fibrations of the $6 \rightarrow 3$ tiling problem corresponding to the first 6-line arrangement are all equivalent because all 6 lines play the same role with respect to the 5 remaining ones. They are represented by the same α in table 3.

Concerning the connectivity problem one can see that it remains only three open cases. One of them corresponds to the first arrangement of 6 lines and so to the icosahedral symmetry. Note that it can bias the issue of few results on the fractions of cyclic base $6 \rightarrow 3$ tilings. Indeed, the corresponding base tiling sets might be non-connected and our Monte Carlo sampling might be incorrect. Actually, a thorough study of 7-line arrangements shows that only two of them hold the first 6-line arrangement, the second and the sixth. In the second 7-line arrangement, this problem appears when we suppress the first or the fifth line, in the sixth one when we suppress the first line.

Cycle abundance in $5 \rightarrow 3$ base tilings fitted by $1 - (1 - \alpha)^{\binom{5}{3}p^3}$								
6-line arrangement number		Particularized line λ_{sup}						Connectivity problem
		1	2	3	4	5	6	
α	1	1.32e-06	1.32e-06	1.32e-06	1.32e-06	1.32e-06	1.32e-06	open
α	2	0	0	0	0	0	0	connected
α	3	0	0	0	0	0	0	connected
α	4	0	0	0	0	0	0	connected

Table 3. Results of the fits of fractions of cyclic tilings by $1 - (1 - \alpha)^{10p^3}$. The zeros represent fibrations where we have proven that cycles cannot appear. All the tiling problems based on first 6-line arrangement with one particularized line are identical, it is why they are represented by the same α . The connectivity problems remains open for this arrangement since it possesses cycles in all its fibrations.

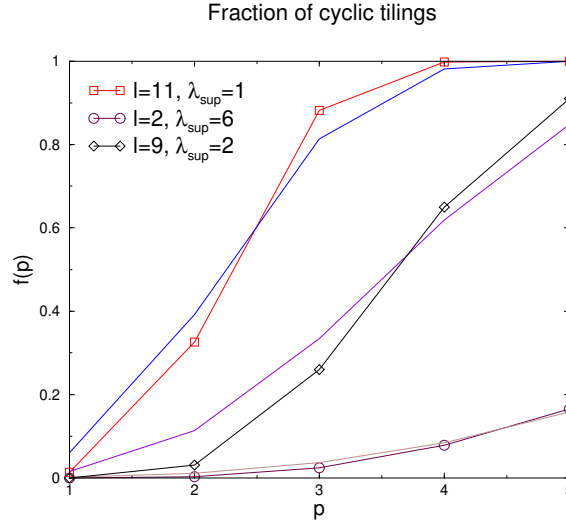


Figure 14. Typical fraction of cyclic tilings (when they are not equal to zero) as a function of boundary size. The curves with squares, diamond and circles are the measured ones, whereas the others are fits with: $1 - (1 - \alpha)^{20p^3}$. We represent only some cycle fractions for $6 \rightarrow 3$ tilings for visibility.

Cycle abundance in $6 \rightarrow 3$ base tilings fitted by $1 - (1 - \alpha)^{20p^3}$								
	7-line arrangement number	Particularized line λ_{sup}						Connectivity problem
		1	2	3	4	5	6	
α	1	0	0	0	0	0	0	connected
α	2	N.A.	2.98e-5	3.57e-5	2.15e-5	N.A.	1.38e-4	1.13e-4
α	3	0	0	0	7.58e-3	0	0	connected
α	4	0	0	0	0	0	0	connected
α	5	0	0	0	0	0	0	connected
α	6	5.93e-3	1.39e-4	3.32e-4	2.81e-4	1.65e-4	1.93e-4	3.18e-4
α	7	0	0	0	2.13e-4	4.05e-4	2.14e-4	0
α	8	5.01e-4	0	0	0	0	0	connected
α	9	0	1.51e-3	0	0	6.86e-3	6.14e-3	0
α	10	0	0	0	0	6.07e-3	0	connected
α	11	6.20e-3	0	0	0	0	0	connected

Table 4. Results of the fits of fractions of cyclic tilings by $(1 - \alpha)^{20p^3}$. The acronym “N.A” holds for non-available: in that cases, we found cycles but not enough for the reliability of the fit. The connectivity problem remains open only for the second and the sixth line arrangements, since for the others we can prove that at least one fibration cannot possess cycles. All configuration sets of $6 \rightarrow 3$ base tiling problems are proven to be connected except the 3 ones written in bold faces.

5.3. Structure of the configuration space

We now make a brief incursion into graph theory and order theory. The configuration space can be seen as a graph G , the vertices of which represent tilings, and the edges of which represent single flips: given two tilings t_1 and t_2 , (t_1, t_2) is an edge of G if t_1 and t_2 differ by (only) one single flip (see figure 5). We prove that this graph G can be embedded in a high-dimensional hyper-cubic lattice L , thus generalizing results

previously specialized to plane octagonal tilings [16], even in the possible case where G is not connected.

As an immediate corollary, we demonstrate that this graph can be given a structure of *graded partially ordered set* (graded “poset”) [37]. Indeed a partial order relation is associated below to the iterated partition-on-tiling process. Saying that this poset is graded means that there exists a *rank function* r on configurations such that if t_1 covers (*i.e.* is just above) t_2 then $r(t_1) = r(t_2) + 1$. This rank function is simply the sum of the (integral) coordinates of a tiling in the lattice L . This order has unique minimal and maximal elements.

The present point of view is applicable to tiling sets of any dimension d and codimension $D - d$.

5.3.1. Structure of the graph

We first prove that the configuration space can be seen as a graph G_D embedded in a high-dimensional hyper-cubic L_D . We proceed by induction on the codimension $D - d$, for any fixed dimension d .

In codimension 1, the tilings are encoded by hyper-cubic partitions. The coordinates of a tiling are simply the K_{d+1} parts x_k , $k = 1, \dots, K_{d+1}$, of its associated partition and a tiling is therefore naturally represented by a point of integral coordinates in a hyper-cubic lattice L_{d+1} of dimension K_{d+1} . A flip is encoded by an increase or decrease of the corresponding part by one unit and thus it corresponds to an edge of the hypercubic lattice.

Suppose now that the above property holds for the graph G_D . A $D + 1 \rightarrow d$ tiling t is encoded by both a $D \rightarrow d$ base tiling \tilde{t} and a generalized partition on this base tiling. By hypothesis, the base tiling is encoded by K_D integral coordinates x_k , $k = 1, \dots, K_D$. We denote by y_l , $l = 1, \dots, K'$ the parts of the partition. We now demonstrate that if t is encoded by the coordinates $(x_1, \dots, x_{K_D}, y_1, \dots, y_{K'})$, then G_{D+1} is embedded in a lattice L_{D+1} of dimension $K_{D+1} = K_D + K'$.

The only subtlety comes from the fact that the indices l must be correctly chosen with respect to the base tiling \tilde{t} , so that G_{D+1} is *globally* embedded in a hyper-cubic lattice (and not only *locally*), as it is already discussed in reference [16] in the special case of octagonal tilings. We do not reproduce the ideas of this reference which cannot be easily generalized.

A tile of any base tiling \tilde{t} is defined as the intersection of d de Bruijn surfaces. The de Bruijn families are indexed by a_1, \dots, a_d and in each family a , the surface is indexed by q_a . A tile is now indexed by the $2d$ indices $(a_1, \dots, a_d, q_{a_1}, \dots, q_{a_d})$ independently of \tilde{t} . We simply fix an arbitrary one-to-one correspondence between these indices and the indices $l = 1, \dots, K'$, independent of the tiling \tilde{t} .

Now that we have defined the integral coordinates of a tiling, we only need to check that both type-I and type-II flips respect the lattice structure, that is to say that they correspond to an increase or a decrease of (only) one coordinate by one unit.

Type-II flips do not affect the base tiling (the x_k are unchanged) whereas they change exactly one y_l by ± 1 ; Type-I flips concern the base tiling only: they change one x_k by ± 1 and $d + 1$ tiles of the base tiling move. Since the flip is possible, they all bear the same part value before the flip. After the flip, these part values remain unchanged. Since the tiles involved in the flip bear the same indices l before and after the flip, the coordinates y_l remain unchanged. To sum up, either one x_k or one y_l (and only one) is increased or decreased by one unit when a flip is achieved.

5.3.2. Structure of graded poset

When G_D is connected by flips, as far as the order structure is concerned, the previous results ensure that G_D has a structure of graded poset inherited from the order structure of L_D : a tiling t_1 is greater than a tiling t_2 if all the coordinates of t_1 are greater than the corresponding coordinates of t_2 in L_D . The rank function $r(t)$ is simply the sum of the coordinates of t in the lattice L_D . The minimum tiling is obtained when all the parts are set to 0. The maximum tiling is obtained when all the parts are set to their maximum possible value. The same kind of result is also established in [36] in codimension 2.

To close this section, note that the existence of the rank function r make in principle possible the application of the technique developed in reference [17] to calculate numerically the entropy of tilings with a given edge orientation, as soon as the configuration space is connected by flips.

6. Numerical study of vertex self-diffusion

In this section, we study vertex self-diffusion in rhombohedra tilings. Even though self-diffusion is only one way of characterizing flip dynamics among many possible ones, we have chosen to focus on this observable because of its physical interest (see section 7 and the end of this section for a discussion on other quantities of interest related to flip dynamics).

Indeed, single flips have a counterpart at the atomic level [38, 39] which is a new source of atomic mobility as compared to usual mechanisms in crystals. Consecutively, flip-assisted atomic self-diffusion has been anticipated as a transport process specific to quasi-crystalline materials [24] which is susceptible to play a role in their mechanical properties, even if it remains controversial whether or not flip-assisted self-diffusion is dominant as compared to usual mechanisms [40].

In addition, quasicrystals present a sharp brittle-ductile transition well above their melting transition (for a review, see Urban *et al.* [41]), which is related to a rapid increase of dislocation mobility [25]. Note that the latter does not seem to be directly associated with any phason unlocking transition because the phason faults dragged behind a moving dislocation are not healed immediately (neither above or below the transition) and the friction force on a dislocation due to the trailing of phason faults should not vary significantly at the brittle-ductile transition [42]. However, dislocation movement by pure climb [43, 44, 42] requires the diffusion of atomic species over large distances. Therefore dislocation mobility is also directly related to atomic self-diffusion.

Here we study the diffusion of vertices in tilings. As it was first established in [24], one must focus on diffusion of vertices rather than diffusion of tiles because tiles cannot travel long distances under flip sequences. Diffusion of vertices is a first approximation before a more realistic and refined approach taking into account atomic decorations of tiles. But the possible effects of cycles we want to address here are already present at the scale of tiles and we shall not consider atomic decorations in this paper.

We demonstrate that cycles do not have any significant influence on self-diffusion, both at the qualitative and quantitative levels.

Before tackling the study of vertex diffusion, we argue that diffusion in fixed-boundary tilings is relevant to the more physical diffusion in free- (or periodic-) boundary tilings provided one focuses on the central regions of the fixed-boundary tilings, where the tilings forget the influence of the polyhedral boundary.

6.1. Diffusion in fixed- versus free-boundary tilings

Since [12], it is known that fixed zonotopal boundaries have a strong influence on rhombus tilings. This boundary sensitivity has been widely studied in two dimensions (see references in [17]) and recently numerically explored in $4 \rightarrow 3$ tilings [10, 17]. This spectacular effect is generically known as the “arctic phenomenon”, which means that at the large size limit, constraints imposed by the boundary “freeze” macroscopic regions near the boundary. In these frozen regions, the tiling is periodic, contains only one tile species, and has a vanishing entropy. By contrast, the remaining “unfrozen” regions contain random tilings with several tile species and have a finite entropy per tile. In the two-dimensional hexagonal case, the unfrozen region is inscribed in an “arctic circle”. The tiling is not homogeneous inside this circle and presents an entropy gradient.

By contrast, in $4 \rightarrow 3$ tilings filling a rhombic dodecahedron, it has been numerically established that the unfrozen region is an octahedron [10, 17], inside which the tiling is homogeneous and the entropy per tile is constant. In other words, inside the octahedron, the tiling is a *free-boundary* one. This octahedron contains $2/3$ of the tiles.

In [17], it is argued that this qualitative difference between two- and three-dimensional tilings is related to the entropic repulsion between de Bruijn lines and surfaces. In dimension 2, it is favorable to bend de Bruijn lines because the bending cost is smaller than the entropy gained by moving lines away. The reverse holds in dimension 3 for de Bruijn surfaces: they are not forced away from their flat configuration and they remain stacked in the octahedron. It is anticipated in [17] that the same kind of result holds in higher codimension three-dimensional tilings: if the de Bruijn surfaces are not forced away from their flat configuration, there should be a large macroscopic central region where all de Bruijn families are present and form a free-boundary tiling, thus forgetting the presence of the polyhedral boundary. For example, a simple calculation shows that in diagonal icosahedral tilings, this region contains about 42% of the tiles.

If one wants to relate vertex diffusion in random tilings to atomic diffusion in real quasicrystals, it is essential to get rid of the non-physical influence of fixed polyhedral boundaries (see the discussion in [17] on this last point). Therefore in the following, we study vertex self-diffusion in this central region: the initial positions of the vertices are chosen in a very small central sphere and we check that their distance to the center never exceeds a finite fraction ($\sim 50\%$) of the tiling shortest radius. As a consequence, we have argued that we study self-diffusion in effectively free-boundary tilings.

Below, we compare diffusion constants in this central region of fixed-boundary icosahedral tilings with the similar constant in tilings with periodic boundary conditions [21]. We find an excellent agreement, which corroborates that the tiling in the central region is effectively a free- (or equivalently periodic-) boundary one and which reinforces our analysis.

6.2. Numerical results

Our purpose here is not to propose an exhaustive study of vertex self-diffusion that was already done in reference [21], but rather to check that cycles have no significant influence on the diffusive behavior. In this section, we also focus on diagonal tilings.

We first present how we implement the numerical studies of vertex self-diffusion.

As we did it in section 5.2, we start with tilings made by flat de Bruijn surfaces and consider the Monte Carlo Markovian dynamics described in section 3. We begin by equilibrating the tiling during a time which scales with the system size as $p^2 \sim N_v^{2/3}$ as it was argued in section 5.2. Typically, for a tiling size $p = 20$ that we present here, the equilibration time is of order 10^5 Monte Carlo sweeps. As we explained it above, we then choose a small central cluster of vertices i for which we follow the position $r_i(t)$ as a function of time. The number of vertices in a central cluster is around 4000 for $p = 20$ whereas the tiling contains more than 10^5 vertices. Each vertex position is recorded on a period of $5 \cdot 10^4$ Monte Carlo sweeps. At each interval of 5000 Monte Carlo sweeps we define a new central cluster of vertices independent of the previous one which gives us new position samples. We use 40 of these samples in the case of $6 \rightarrow 3$ tilings and 25 in the case of $7 \rightarrow 3$ tilings.

We compute the mean square displacement averaged over all vertices and all samples: $\langle (r(t) - r(0))^2 \rangle$. The results displayed in figures 15 and 16 are normalized by the mean square displacement of a vertex during a single flip averaged over the time, the vertices and the samples: $\langle s^2 \rangle$. Indeed the diffusion constant κ of a standard random walker making independent steps reads: $\kappa = \langle s^2 \rangle / \tau_0$, where τ_0 is a typical time between two steps and $\langle s^2 \rangle$ the typical square distance covered by the walker at each step. Here, the mean square displacement of the vertices also naturally depends on the typical distance covered at each flip. This distance depends on which line arrangement the orientation vectors are based, but also on how they are geometrically built from a line arrangement, since we have a liberty of choice of edge orientations among the same equivalent class. The normalization coefficient, $\langle s^2 \rangle$, smooths the differences between orientation vectors inside an equivalent class.

Nevertheless, the vertex displacement cannot be considered as the displacement of a standard random walker on a lattice. There certainly exists a lot of correlations in vertex displacements [21], and as we will see it below, the typical time which arises from the diffusion constant is larger than a Monte Carlo sweep. The normalized diffusion constant we found for different edge orientations in a same equivalent class (namely the second 6-line arrangement) shows that this normalization is not sufficient. The order of magnitude of the differences between these diffusion constants in a same equivalence class was of the same order as those between different classes. So we are not able to compare quantitatively the differences in the diffusion dynamics between two classes. We display quantitative results in the case of icosahedral symmetry where orientation vectors are well defined. In this case we find normal diffusion with a not normalized diffusion constant $\kappa = 0.0013$, which is very close to the one found in reference [21] in the case of periodic-boundary tilings.

But the aim of this study was more to observe the possible fundamental differences in flip dynamics between tilings with and without cycles. In particular to check if anomalous diffusion arises in tilings with cycles. The results shown in figures 15 and 16 present no anomalous diffusion whatever the tiling we are considering. For each arrangement, the mean square displacement exhibits a transition regime before the diffusive one because of short-time correlations. This regime stops around $\langle (r(t) - r(0))^2 \rangle / \langle s^2 \rangle \sim 1$. One can interpret the duration of this transient regime as the typical time τ_0 between two uncorrelated flips. Indeed, a vertex just being flipped can only be flipped again to its initial position at the next step. To have large distances covered by a vertex, the flip of this vertex has to be followed by a collective sequence of vertex flips around it. During this flip sequence, the vertex goes through an unflippable configuration to a new flippable one which can be different from the

initial one. This collective succession of flips should take a time of order τ_0 . This time τ_0 is found to lie between 500 and 1000 MCS in all the cases studied here.

We now briefly discuss a possible reason why cycles should have no influence on the dynamics, even if they are very abundant for some line arrangements at a size $p = 20$. We have seen in section 3 that disconnected fibers based on tilings with cycles are necessarily a lot smaller than the connected ones without cycles. Which means that tilings in disconnected fibers should not be necessarily dominant even if such fibers are themselves dominant. The configuration spaces are sketched as in figure 6, with a large majority of small fibers and a minority of big ones. The influence of cycles might be a competition between the proportion of small fibers and their size. In a mean-field point of view, the sizes of fibers vary as $\exp(N_{eff}S_0)$, as it was argued in section 3, and the proportion of connected fibers as: $(1 - \alpha)^{N_T} \simeq \exp(-\alpha N_T)$. The proportion of disconnected fibers tends to 1. If the number of effective parts in cyclic base tilings is proportional to the number of tiles: $N_{eff} \sim \beta N_T$, the number of tilings in *disconnected* fibers grows as

$$\mathcal{N}_{nc} \sim \exp(\beta S_0 N_T) \quad (4)$$

whereas the number of tilings in *connected* fibers is

$$\mathcal{N}_c \sim \exp((S_0 - \alpha) N_T). \quad (5)$$

Thus, the preponderance of one over the other will depend on the precise values of β , S_0 , and α . If $\mathcal{N}_c \gg \mathcal{N}_{nc}$, the system will spend most of its time in connected fibers and might not see cycles. Unfortunately these quantities are difficult to extract numerically, as well as analytically and we cannot conclude definitively.

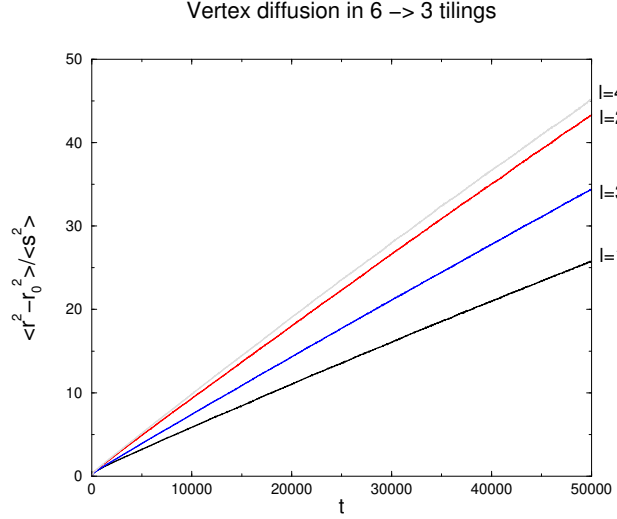


Figure 15. Normalized mean square displacement of vertices in $6 \rightarrow 3$ tilings with $p = 20$. For all line arrangements we find normal diffusion after a transient.

To close this section, we mention that the study of diffusion enables a rough estimate of ergodic times in tiling sets. We recall that the ergodic time τ of a Markovian process is the typical time the process needs to reach stationarity, in other words to be likely to have reached any configuration with nearly equal probability.

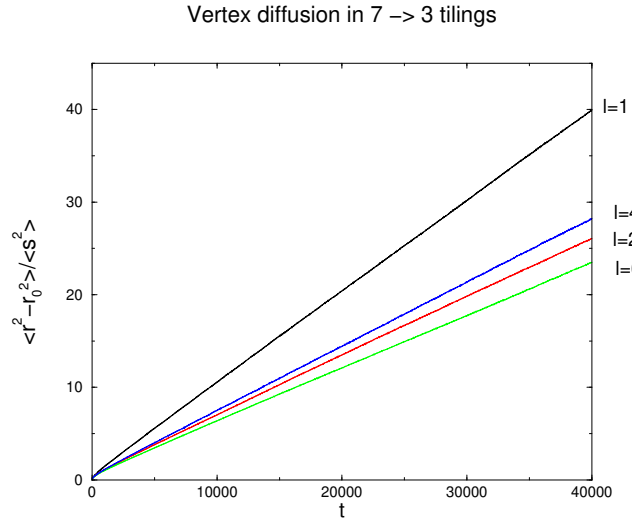


Figure 16. Characteristic normalized mean square displacement of vertices in $7 \rightarrow 3$ tilings with $p = 20$. The arrangements $l = 1$ and $l = 4$ correspond to tilings without cycles in any fibrations whereas for $l = 2$ and $l = 6$ they correspond to tilings with cycles in all fibrations. For all line arrangements we find normal diffusion after a transient.

A time scale can be associated with vertex diffusion, and is related to the approach of stationarity: it is the typical time needed by a vertex to explore the whole tiling, namely $\tau \sim p^2/\kappa$ for a tiling of typical radius p . This time is compatible with known ergodic times in dimension 2 [33, 26] and in $4 \rightarrow 3$ tilings [10].

7. Conclusion and outlooks

This paper studies sets of three- (and higher-) dimensional tilings by rhombohedra endowed with local rearrangements of tiles called elementary flips or localized phasons. It uses a coding of tilings by generalized partitions which turns out to be a powerful tool to prove connectivity by flips in a large variety of cases. These results answer positively (even though partially) an old conjecture of Las Vergnas [27].

The general idea of the proof is as follows: consider a tiling problem of codimension c . We intend to prove the connectivity of its configuration space G_c . The generalized partition-on-tiling point of view provides a natural decomposition of G into disjoint *fibers* above a *base*. The base is the configuration space G_{c-1} of a tiling problem of codimension $c-1$. Therefore if it can be proven inductively that the latter configuration space G_{c-1} is connected *and that all fibers are connected*, the overall connectivity of G_c follows.

So far, attempts of proofs of connectivity have failed because of the possible existence of cycles in generalized partition problems. As it is discussed in the paper, these cycles block locally some type of flips, the proof of connectivity of fibers *a priori* fails and the simple iterative proof of overall connectivity fails in its turn. What we demonstrate in this paper is that this problem can be bypassed in a large majority of cases because, in general, there exists one way of implementing the generalized

partition (one “fibration”) so that it does not generate cycles. As a consequence, fibers are connected. Since it can also be proven inductively that the *base* is connected, the overall connectivity can be established.

We say “a large majority of cases” because the result depends on the choice of edge orientations. Indeed, we address in this paper the implications in random tiling theory and quasicrystal science of this issue. For example, beside the usual orientation of edges associated with the icosahedral symmetry, there exist 3 additional non-equivalent choices of edge orientations for codimension-three tilings. This means that we consider tilings with the same amount of different tile species (namely 20), but the sets of tiles are non-equivalent in that sense that the tilings they generate cannot be put in one-to-one correspondence. It happens that cycles exist only in the icosahedral case but cannot exist in the three remaining cases. As a consequence, the only codimension-three case where we cannot establish connectivity is the icosahedral one. Similarly, there are 11 non-equivalent edge orientations in codimension 4 and we prove connectivity in all of them except 2. Note that the fixed polyhedral tiling boundaries generated by the generalized partition method also depend on the edge orientations. But these boundaries are not a central issue since we argue in the paper that there exists a large central region where the tiling is effectively a free-boundary one.

The counterparts of cycles at the tiling level are clusters of tiles that are more difficult to break by flips than the remainder of the tiling because some type of flips is locally absent. It was legitimate to anticipate that they might be responsible for entropic barriers and slow down flip dynamics. We have chosen to address the possible effects of cycles on flip dynamics from the angle of vertex self-diffusion because it is a key issue at the physical level. We prove in this paper that there exist tiling problems of the same codimension with (i) no cycles in any fibration; (ii) cycles in some fibrations but not all of them; (iii) cycles in all fibrations. Connectivity holds in cases (i) and (ii) and remains open in case (iii). We compared self-diffusion in the extreme cases (i) and (iii), and we did not detect any significant effect such as a sub-diffusive regime. Therefore even if cycles break connectivity in case (iii), they do not affect significantly the diffusive properties of physical interest.

The tilings considered here have non-physical fixed boundaries. However, we have argued that a macroscopic part of tilings can be considered as a free-boundary one. In addition, we know that $4 \rightarrow 3$ base tilings cannot generate cycles. Therefore the cycles detected in base $5 \rightarrow 3$ tilings (in relation with $6 \rightarrow 3$ ones) cannot but appear in this central region which is effectively of $5 \rightarrow 3$ type and not in the peripheral ones of effective $3 \rightarrow 3$ or $4 \rightarrow 3$ type. Therefore the possible influence of cycles on the dynamics of fixed-boundary $6 \rightarrow 3$ tilings would be reminiscent of such effects on free-boundary $6 \rightarrow 3$ tilings. Since no such effect was detected, we see that our results can be legitimately transposed to free-boundary tilings.

Beyond diffusive properties, flip dynamics can be characterized by the calculation of ergodic times (the times needed to reach stationarity in the flip Markovian process). We have not addressed this question in the paper. The only conclusion that we can draw is that a diffusive behavior is compatible with ergodic times quadratic in the system size. This point will have to be clarified in the future, but beyond numerical techniques, the methods to tackle this point ought to be invented. The standard methods in this field cannot easily be adapted because of the existence of cycles which make impossible the calculation of these times in some fibers that are not connected any longer.

Another issue that is not addressed in this paper is the influence of energy interactions between tiles at finite temperature. More realistic tiling models take into account a tile Hamiltonian (reminiscent of interactions at the atomic level) that favors a quasicrystalline order at low temperature. We intend to analyze the effects of cycles in this context in a future work.

To finish with, we mention that the possible influence of cycles can be quantified on other observables than vertex self-diffusion. For example, we have explored in a preliminary work how the part values X_u converge towards their average value. The part value in the generalized partition formalism is an indication of the position of a tile in the tiling. A deviation in the limiting values would mean that some tiles do not find easily their equilibrium positions in the tiling. It would be a manifestation of ergodicity (or even connectivity) breaking. In general the convergence is rapid. However, we have observed in rare circumstances in the case (iii) above that these values do not converge exactly to their expected equilibrium limit. But in the state of progress of this work, it would be premature to draw any conclusion because we are not able yet to distinguish definitively between a real effect and statistical noise. This work is in progress.

Acknowledgments

One of us (ND) is indebted to Victor Reiner for making him aware of the existence of cycles and of non-equivalent edge orientations in dimension 3. We also express our gratitude to Rémy Mosseri, Éric Rémila and Daniel Caillard for fruitful discussions and debates.

Appendix A. Connectivity of codimension 1 and 2 tiling sets in any dimension

In this appendix, we prove connectivity of sets of codimension-1 and 2 rhombus tilings of any dimension d . In codimension 1, the proof is immediate since such tilings are coded by (acyclic) hyper-solid partitions [15] and since we prove in Appendix B that they are consequently connected. In codimension 2, we also use a proof by monotony as in section 5, even if we do not work directly on hyper-plane arrangements in the projective space \mathbb{PR}^{d-1} . Note that all edge orientations are equivalent in any dimension and codimensions 1 and 2 [45].

We code $d+2 \rightarrow d$ tilings as generalized partitions on $d+1 \rightarrow d$ codimension-one tilings. For sake of convenience, we identify \mathbb{R}^d with the hyperplane H_d of \mathbb{R}^{d+1} of equation $\sum x_i = 0$ and we choose the $d+1$ vectors \mathbf{e}_a as follows:

$$\begin{aligned} \mathbf{e}_1 &= (-d, 1, \dots, 1), \\ \mathbf{e}_2 &= (1, -d, 1, \dots, 1), \\ &\vdots \quad \vdots \quad \vdots \\ \mathbf{e}_d &= (1, \dots, 1, -d), \\ \mathbf{e}_{d+1} &= (-1, -1, \dots, -1, d). \end{aligned} \tag{A.1}$$

The $(d+2)$ -th orientation which orients base $d+1 \rightarrow d$ tilings is chosen as

$$\mathbf{e}_{d+2} = (-1 + \epsilon, -1 + \epsilon^2, \dots, -1 + \epsilon^d, d - (\epsilon + \dots + \epsilon^d)), \tag{A.2}$$

where ϵ is a small positive parameter. This choice is a convenient one among any (non-degenerate) other one because all edge orientations are equivalent in codimension 2 [45]. A face of a base tiling \tilde{t} is oriented accordingly to e_{d+2} . Now we exhibit precisely the orientation of each face species.

A face species is defined by $d-1$ edge orientations among the $d+1$ possible ones. We denote by a and b , $a < b$, the two indices of the edge orientations that do *not* define a face species, and by \mathcal{F}_{ab} this face species. We also denote by \mathbf{g}_{ab} the vector normal to the faces \mathcal{F}_{ab} . A simple calculation shows that

$$\mathbf{g}_{ab} = (0, \dots, 0, 1, 0, \dots, 0, -1, 0, \dots, 0), \quad (\text{A.3})$$

where the non-zero coordinates are in positions a and b . We define $\hat{\mathbf{g}}_{ab} = +\mathbf{g}_{ab}$ when $b \neq d+1$ and $\hat{\mathbf{g}}_{ab} = -\mathbf{g}_{ab}$ when $b = d+1$. Then $e_{d+2} \cdot \hat{\mathbf{g}}_{ab} > 0$ for any a and b : a face \mathcal{F}_{ab} is oriented positively in the direction $\hat{\mathbf{g}}_{ab}$, as far as the order relation between the tiles it separates is concerned.

In addition, $e_{d+1} \cdot \hat{\mathbf{g}}_{a,d+1} > 0$ whatever $a < d+1$, which proves that e_{d+2} and e_{d+1} are companion vectors, which in turn proves the monotony of the de Bruijn indices q_{d+1} with respect to the order between tiles. The connectivity follows as in section 5.

Appendix B. Connectivity of a fiber when the base tiling is acyclic

In this section, we demonstrate that when a base tiling (or more generally a generalized partition problem) is acyclic, the corresponding fiber is connected. We prove that any partition x can be connected to the minimum partition z where all parts are set to 0.

We proceed by induction on the sum $\sigma(x)$ of the parts of x . Suppose the result holds for all x such that $\sigma(x) \leq \sigma_0$. Consider a partition y with $\sigma(y) = \sigma_0 + 1$.

Among all the parts of y bearing non-zero parts, consider a minimal one with respect to the order between parts. Such a part exists because of the acyclic character of the partition problem. Set this part to 0 by successive single flips. The so-obtained partition y' is connected to z because $\sigma(y') \leq \sigma_0$, which proves that y is connected by flips to z .

References

- [1] D. Levine, P.J. Steinhardt, Quasicrystals: a new class of ordered structure, *Phys. Rev. Lett.* **53**, 2477 (1984).
- [2] V. Elser, Comment on “Quasicrystals: a new class of ordered structures”, *Phys. Rev. Lett.* **54**, 1730 (1985).
- [3] C.L. Henley, Random tiling models, in *Quasicrystals, the State of the Art*, Ed. D.P. Di Vincenzo, P.J. Steinhardt (World Scientific, 1991), 429.
- [4] R. Penrose, The role of aesthetics in pure and applied mathematical research, *Bull. Inst. Math. Appl.* **10**, 226 (1974).
- [5] R. Kenyon, Tiling a polygon with parallelograms, *Algorithmica* **9**, 382 (1993).
- [6] S. Elnitsky, Rhombic tilings of polygons and classes of reduced words in Coxeter groups, *J. Combinatorial Theory A* **77**, 193–221 (1997).
- [7] *Tilings of zonotopes: Discriminantal arrangements, oriented matroids, and enumeration*, G.D. Bailey, Ph. D. Thesis (Univ. of Minnesota, 1997).
- [8] H. Cohn, M. Larsen, J. Propp, The shape of a typical boxed plane partition, *New York J. of Math.* **4**, 137 (1998).
- [9] H. Cohn, R. Kenyon, J. Propp, A variational principle for domino tilings, *J. of the AMS* **14**, 297 (2001).
- [10] J. Linde, C. Moore, M.G. Nordahl, An n -dimensional generalization of the rhombus tilings, in *Proceedings of the Conference DM-CCG: Discrete Models: Combinatorics, Computation, and Geometry* (Paris, 2001), p. 23.

- [11] M. Duneau, A. Katz, Quasiperiodic patterns, *Phys. Rev. Lett.* **54**, 2688 (1985); A.P. Kalugin, A.Y. Kitaev and L.S. Levitov, $Al_{0.86}Mn_{0.14}$: a Six-Dimensional Crystal, *JETP Lett.* **41**, 145 (1985); A.P. Kalugin, A.Y. Kitaev and L.S. Levitov, 6-Dimensional Properties of $Al_{0.86}Mn_{0.14}$, *J. Phys. Lett. France* **46**, L601 (1985).
- [12] V. Elser, Solution of the dimer problem on a hexagonal lattice with boundary, *J. Phys. A: Math. Gen.* **17**, 1509 (1984).
- [13] R. Mosseri, F. Bailly, C. Sire, Configurational entropy in random tiling models, *J. Non-Cryst. Solids*, **153&154**, 201 (1993).
- [14] R. Mosseri, F. Bailly, Configurational entropy in octagonal tiling models, *Int. J. Mod. Phys. B*, Vol 7, **6&7**, 1427 (1993).
- [15] N. Destainville, R. Mosseri, F. Bailly, Configurational entropy of codimension-one tilings and directed membranes, *J. Stat. Phys.* **87**, 697 (1997).
- [16] N. Destainville, R. Mosseri, F. Bailly, Fixed-boundary octagonal random tilings: a combinatorial approach, *J. Stat. Phys.* **102**, 147 (2001).
- [17] M. Widom, R. Mosseri, N. Destainville, F. Bailly, Arctic octahedron in three-dimensional rhombus tilings and related integer solid partitions, *J. Stat. Phys.* **109**, 945 (2002).
- [18] *Regular Polytopes*, H.S.M. Coxeter (Dover, 1973).
- [19] L.-H. Tang, Random-tiling quasicrystal in three dimensions, *Phys. Rev. Lett.* **64**, 2390 (1990).
- [20] L.J. Shaw, V. Elser, C.L. Henley, Long-range order in a three-dimensional random-tiling quasicrystal, *Phys. Rev. B* **43**, 3423 (1991).
- [21] M.V. Jarić, E. Sørensen, Self-diffusion in random-tiling quasicrystals, *Phys. Rev. Lett.* **73**, 2464 (1994).
- [22] F. Gähler, in *Proceedings of the fifth international conference on quasicrystals*, Eds. C. Janot and R. Mosseri (World Scientific, Singapore, 1995), p. 236.
- [23] W. Ebinger, J. Roth, H.R. Trebin, Properties of random tilings in three dimensions, *Phys. Rev. B* **58**, 8338 (1998).
- [24] P.A. Kalugin, A. Katz, A mechanism for self-diffusion in quasi-crystals, *Europhys. Lett.* **21** (9), 921 (1993).
- [25] M. Wollgarten, M. Beyss, K. Urban, H. Liebertz, U. Köster, Direct evidence for plastic deformation of quasicrystals by means of a dislocation mechanism, *Phys. rev. Lett.* **71**, 549 (1993).
- [26] N. Destainville, Flip dynamics in octagonal rhombus tiling sets, *Phys. Rev. Lett.* **88**, 30601 (2002).
- [27] M. Las Vergnas, Convexity in oriented matroids, *J. Comb. Theory Ser. B* **29**, 231 (1980).
- [28] N.G. de Bruijn, Algebraic theory of Penrose's non-periodic tilings of the plane, *Kon. Nederl. Akad. Wetensch. Proc. Ser. A* **84** (1981) 1-38.
- [29] N.G. de Bruijn, Dualization of multigrids, *J. Phys. France* **47** (1986) C3-9.
- [30] *Oriented matroids*, A. Björner, M. Las Vergnas, B. Sturmfels, N. White, G.M. Ziegler (Cambridge University Press, 1993).
- [31] B. Sturmfels, G.M. Ziegler, Extention spaces of oriented matroids, *Discrete & Computational Geom.* **10**, 23 (1993).
- [32] K.J. Strandburg, P.R. Dressel, Thermodynamic behavior of a Penrose-tiling quasicrystal, *Phys. Rev. B* **41**, 2469 (1990).
- [33] D. Randall and P. Tetali, Analyzing Glauber dynamics by comparison of Markov chains, *J. Math. Phys.* **41** (3), 1598 (2000).
- [34] *Lectures on Polytopes*, G.M. Ziegler (Springer-Verlag, 1995).
- [35] *Convex Polytopes*, B. Grünbaum (Interscience Publishers, 1967).
- [36] F. Chavalon, E. Rémy, Rhombus tilings: decomposition and space structure, *preprint*, Tech. report of ENS Lyon, RR2004-30 (2004).
- [37] *Introduction to Lattices and Order*, 2nd edition, B. A. Davey, H. A. Priestley (Cambridge University Press, 2002).
- [38] G. Coddens, C. Soustelle, R. Bellissent, Y. Calverac, Study of hopping in perfect icosahedral $AlFeCu$ quasi-crystal by inelastic neutron scattering, *Europhys. Lett.* **23**, 33 (1993).
- [39] S. Lyonnard, G. Coddens, Y. Calvayrac, D. Gratias, Atomic (phason) hopping in perfect icosahedral quasicrystals $Al_{70.3}Pd_{21.4}Mn_{8.3}$ by time-of-flight quasielastic neutron scattering, *Phys. Rev. B* **53**, 3150 (1996).
- [40] R. Blüher, P. Scharwaechter, W. Frank, H. Kronmüller, First low-temperature radiotracer studies of diffusion in icosahedral quasicrystals, *Phys. Rev. Lett.* **80**, 1014 (1998).
- [41] K. Urban, M. Feuerbacher, M. Wollgarten, M. Bartsch, U. Messerschmidt, in *Physical Properties of Quasicrystals*, ed. Z.M. Stadnik, *Solid State Science* **126**, Springer, 361 (1999).
- [42] D. Caillard, F. Mompou, private communication (2004).

- [43] D. Caillard, F. Mompiou, L. Bresson, D. Gratias, Dislocation climb in icosahedral quasicrystals, *Scripta Mater.*, **49**, 11 (2003).
- [44] F. Mompiou, L. Bresson, P. Cordier, D. Caillard, Dislocation climb and low-temperature plasticity of an Al-Pd-Mn quasicrystal, *Phil. Mag.* **83**, 3133 (2003).
- [45] E. Rémila, private communication (2003). The proof is based upon an argument of duality in the context of oriented matroid theory that is beyond the scope of this paper.